Article

Not peer-reviewed version

Thermo-Viscoelastic Behavior of Antifriction Polymeric Materials

Anna A. Kamenskikh * , Anastasia P. Bogdanova , Yuriy O. Nosov , Yulia S. Kuznetsova

Posted Date: 26 May 2026

doi: 10.20944/preprints202605.1707.v1

Keywords: PTFE; UHMWPE; composite material; foundry coke; carbon fiber; bronze; modification; temperature; viscoelasticity; model

Article

Thermo-Viscoelastic Behavior of Antifriction Polymeric Materials

Anna A. Kamenskikh [1,*], Anastasia P. Bogdanova [1,2], Yuriy O. Nosov [1,2] and Yulia S. Kuznetsova [1,2]

[1] Department of Computational Mathematics, Mechanics and Biomechanics, Perm National Research Polytechnic University, 614990 Perm, Russia

[2] Laboratory of Digital Engineering of Mechanical Engineering Processes and Production, Perm National Research Polytechnic University, 614990 Perm, Russia

* Correspondence: anna_kamenskih@mail.ru; Tel.: +7(342)239-15-64

Abstract

Five modifications of polytetrafluoroethylene (PTFE) are considered as a modern alternative to PTFE as sliding layers of bridge bearing parts. Radiation-modified PTFE without additives and with nano-additives, as well as composites based on PTFE with bronze inclusions and nanomodified carbon fiber fillers, were investigated. Ultra-high-molecular-weight polyethylene (UHMWPE) and classic pure PTFE were considered as control samples. The thermomechanical properties of the materials were studied within the framework of dynamic mechanical analysis in the operating temperature range of bridge structures [−40; +80] °C. The exit zones from the linear theory of viscoelasticity were established for all the materials considered. Temperature dependencies of the storage module and the loss module were determined. Thermo-viscoelastic models of material behavior were constructed using a numerical identification procedure, experimental data, and simulation models. The thermomechanics of materials during the deformation of the spherical support part of the bridge were analyzed. Temperature dependencies of the parameters of the contact stress-strain state were determined with an average coefficient of determination $R^2 = 0.97$ and an average error size RMSE = 0.092.

Keywords: PTFE; UHMWPE; composite material; foundry coke; carbon fiber; bronze; modification; temperature; viscoelasticity; model

---

1. Introduction

Polymers are used in various city-forming industries, such as: construction [1], transport [2], medicine [3,4], oil and gas industry [5], etc. Changing production and solving environmental problems associated with their use lead to the development of types of materials and the expansion of their application in various industries [6–8]. Modern polymer materials differ in properties in different aspects: mechanical, physical, chemical, and technological.

The mechanical properties of polymers depend on the degree of change in their structure, composition, size, and shape, as well as on temperature and mechanical loading [9]. It is necessary to evaluate the functional properties of materials when they are used in various designs [10]. Experimental studies are the main ones at the stage of material selection. Heat resistance, mechanical strength, and wear resistance determine the key properties of structural materials. Their applicability in products also depends on the ambient temperature and thermal loads in general [11]. The glass transition temperature is a fundamental characteristic of amorphous and semi-crystalline polymers, which determines the boundaries of the state of the material: from solid to highly elastic. It significantly affects the scope of the material, making it possible to assess the elasticity and flexibility of polymer products according to temperature limits. The transition to the glassy state usually occurs in a wide range of temperatures [12]. The value of the glass transition/softening temperature Tg

 doi:10.20944/preprints202605.1707.v1

depends on the heating/cooling rate of the sample, as well as on the complex effect of temperature and load [13,14]. The transition to a highly elastic state changes the processes of friction and wear, as a rule, worsening the strength and wear resistance of the polymer [15–17]. Temperature is one of the main factors affecting the properties of polymer and composite materials based on them [18,19]. However, it is the combined effect of temperature and force loads that to a greater extent affects the thermomechanical properties [20].

In this paper, attention is paid to polymer materials used in the bridge construction industry as antifriction layers of thorn nodes (support, bearing). Their work is due to a decrease in friction between steel structural elements, which reduces the wear of parts and increases the service life of bridge structures. The loading rate, strain amplitude, friction coefficient, and temperature regime have been identified as the key parameters affecting the operation of the bearing [21]. The study [22] showed that a decrease in the efficiency of bearings at low temperatures may be the result of the combined effects of low temperature and deformation. Taking into account the thermal effect and conducting temperature monitoring are extremely important at the design stage of elements of bridge structures [23]. In [24], the authors indicate the need to take into account the temperature dependence of the characteristics of the plain bearings under the seismic loads of insulated bridges, since otherwise, the risk of damage will be significantly underestimated. Experimental studies show a significant relationship between the mechanical characteristics of the bearing and the ambient temperature [25], including under cyclic loads [26,27]. In general, temperature has a strong effect on both the properties and the evolution of the stress-strain state of products made of polymer materials [15,28], which in turn determines the main focus of the current study.

Qualitative construction of a numerical analog of the structure, including: analysis of the finite element mesh, settings for the convergence of the solution of a nonlinear problem, selection of a model of material behavior, is necessary to assess the stress-strain state of important nodes [29]. Conducting a wide range of experiments will make it possible to evaluate the fundamental aspects of the behavior of the material. This will identify areas that affect the performance of the structure from the point of view of their modeling. Accurate knowledge of material properties over a wide temperature range is extremely important in numerical modeling. The accumulation of information on the behavior of materials is necessary for the development of modern methods for assessing and predicting the physical characteristics of polymers [30,31]. Due to the complexity of the mechanisms of deformation of polymer materials, mathematical models of behavior description are also developing quite strongly: elastic-plastic [32], viscoelastic-plastic [33,34], and viscoelastic models [35,36]. The identification of model parameters for numerical implementation is often reduced to an optimization problem [37]. However, there are also modern approaches based on neural networks and machine learning [38,39]. This paper presents the results of an experimental study to determine the physical and mechanical properties of a set of modern antifriction materials. The parameters of the viscoelastic model with the decomposition of the relaxation core by the Prony series were identified. A numerical analog of the structure of the support part of the bridge under force loading conditions, taking into account the temperature, was built. The results obtained are necessary for future studies of the behavior of the support part of the bridge under cyclic loading. They will make it possible to formulate recommendations for the use of modern polymers as an antifriction layer in critical friction units under various loads and temperatures. This will ensure compliance with the main criteria for the selection of materials at the stage of designing structures.

2. Materials and Methods

2.1. Materials

Polytetrafluoroethylene (PTFE) was first synthesized in 1938 by Roy Plunkett and is still considered to be the "king of plastics" [40,41]. PTFE (fluoroplastic, Teflon) earned its title of "king" due to its chemical inertness, hydrophobicity, low surface energy, and resistance to thermal, biological, and oxidative decomposition, as well as a low coefficient of friction. Its chemical structure consists of a carbon skeleton surrounded by a protective layer of fluorine atoms [42]. PTFE shows a high degree of structural regularity, which can initiate a greater degree of crystallization of the microstructure, especially at negative temperatures. PTFE exhibits a viscoelastic nature [43]. Plastic deformation of the material, poor thermal stability, and a large coefficient of thermal expansion (CTE) are also noted as features of the thermomechanical behavior of the material [44,45]. The service life of PTFE products, coatings, and interlayers depends on environmental conditions, mechanical, thermal loads, including cyclic ones, as well as the influence of corrosive media [46].

Progress in the field of materials science has made it possible to form a fairly large set of alternatives to the "king of plastics". Ultra-high-molecular-weight polyethylenes (UHMWPE) are one of its competitors [47]. Modifications and composites based on PTFE and UHMWPE are also widespread [48,49]. A set of modern anti-friction nanomodified and nanofilled materials based on PTFE of Russian and Belarusian production is considered as an alternative to widespread materials of sliding layers of bridge bearing parts.

Materials of the Arflon line (Scientific and Production Enterprise "Arflon" LLC, Moscow, Russia) are considered as an alternative to pure PTFE. They are obtained by the method of compacting pure and/or additive-filled PTFE powder, followed by high-temperature radiation treatment. In this study, three basic brands of Arflon are considered: AR-200, AR-202, and AR-204. All of them are based on PTFE powder and modified according to a single technological mode with a degree (dose) of modification 2. The specific parameters of the technological process are not disclosed by the manufacturer.

AR-200 is a structurally modified PTFE without fillers, white, translucent material. According to the manufacturer, it has improved wear resistance, radiation resistance, and heat resistance, as well as a decrease in creep and friction coefficient. The material is recommended for tribotechnical products.

Composite materials produced by Arflon contain finely dispersed organic and inorganic fillers. After pressing, they are also subjected to high-temperature physicochemical modification. AR-202 and AR-204 differ in the type of nanofiller: foundry coke and carbon fiber, respectively. The mass fraction of the filler is 20% in both materials, making them black in color. They are also recommended for tribosystem parts.

Composite Superfluvis SF-1 developed by Grodno Mechanical Plant JSC (Grodno, Republic of Belarus) and the Institute of Mechanics of Metal-Polymer Systems named after V. A. Bely of the National Academy of Sciences of Belarus (Gomel, Republic of Belarus) is considered a promising material for antifriction coatings and layers [49]. The SF-1 material is manufactured on the basis of PTFE using plasma-modifiedcarbon fiber. Approximately 17% of the total weight falls on the modified crushed carbon fiber, the surface of which is coated with a fluoropolymer (nanocoating up to 40 nm thick).

Also, for comparative analysis, the article considers three materials widely used as sliding layers of bridge bearing parts: PTFE; PTFE-based composite material with 40% bronze dendritic inclusions and 2% molybdenum disulfide (F4Br40M2); ultra-high molecular weight polyethylene (UHMWPE). Materials were obtained on the basis of the production company AlfaTech LLC (Perm, Russia).

All of the materials in question are suitable in one way or another as relatively thin, flat, and spherical sliding layers of bridge bearing parts. The thermomechanical properties of materials require analysis, since the structures operate in a wide range of operating temperatures.

2.2. Experiment

Dynamic mechanical analysis (DMA) is selected to determine the thermo-viscoelastic properties of materials. Rectangular samples L×B×H (Figure 1) were studied according to the three-point bending scheme (Figure 2) in the temperature range from −40 °C to +80 °C. DMA Q800 (TA Instruments; New Castle; Delaware; USA) was used to conduct a series of experiments.

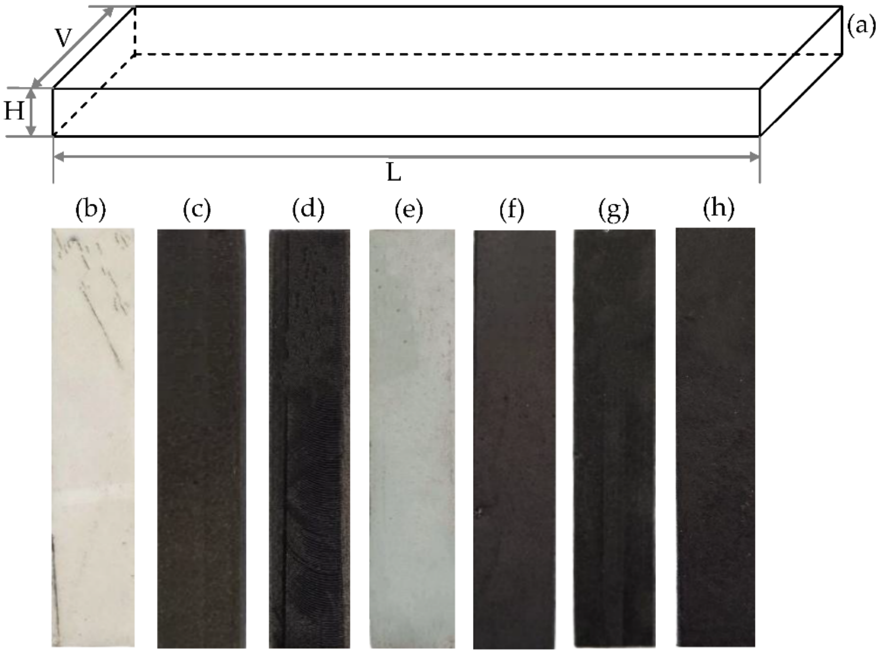

Figure 1. Samples: a is a geometric configuration; b is PTFE; c is F4Br40M2; d is UHMWPE; e is AR-200; f is AR-202; g is AR-204; h is SF-1.

Samples were made by AlfaTech LLC from industrial blanks of sliding layers of bridge bearing parts. Five samples from each material were made for experiments. Geometrical dimensions of the specimens: $L = 59.99 \pm 0.49$ mm, $B = 11.95 \pm 0.13$ mm, and $H = 3.08 \pm 0.11$ mm.

The linear viscoelasticity zone was determined using one sample. This made it possible to establish the amplitudes and deformations near the exit zone from the linear theory of viscoelasticity (Table 1), which were used in the main experiment.

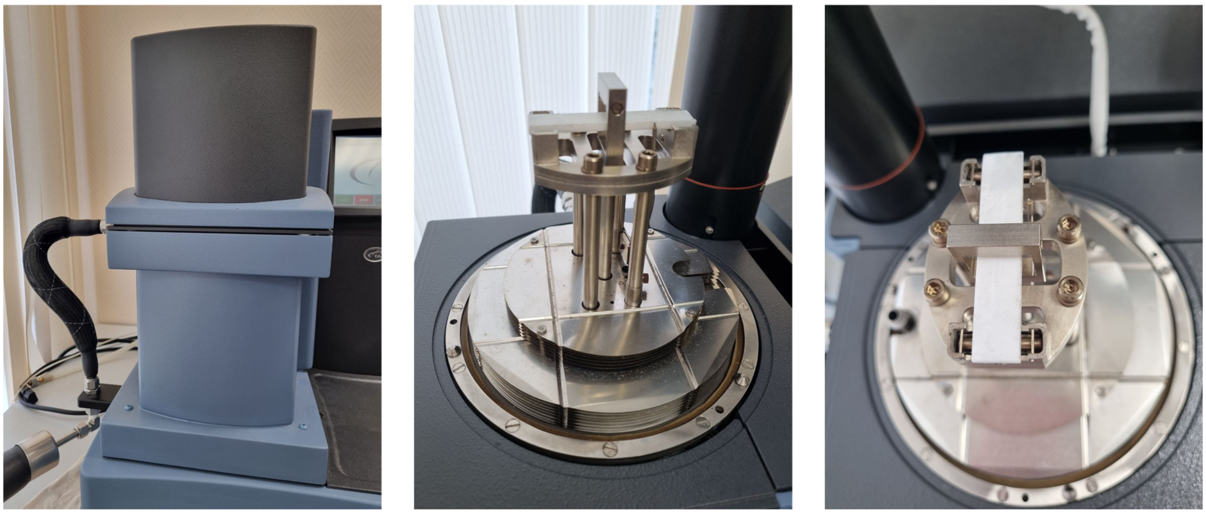

(a) (b) (c)

Figure 2. Dynamic mechanical analysis: a is DMA Q800; b, c are three-point bending of rectangular samples.

Table 1. The parameters near the exit zone from the linear theory of viscoelasticity.

Material	PTFE	F4Br40M2	UHMWPE	AR-200	AR-202	AR-204	SF-1
Amplitude, μm	40	40	150	175	100	75	45
Strain, %	0.0275	0.0275	0.1031	0.1203	0.0688	0.0516	0.0309

The experiment was carried out in two stages: 1) heating the sample to +80 °C for 20 minutes with exposure at a given temperature for 10 minutes; 2) oscillating load near the exit zone from the linear theory of viscoelasticity with a frequency of 1 Hz with gradual cooling to −40 °C and a rate of change of 2 °C/min.

During the experiment, the temperature dependence of the storage module, the loss module, and the tangent of the angle of mechanical losses was recorded. For static significance of the results, the experiment was repeated 4 times for each material. This also provides an analysis of the homogeneity of the properties of the materials in the industrial blanks of the sliding layers.

2.3. Constitutive Model of the Material

The general equation of a linear viscoelastic material has the form:

$$\boldsymbol{\sigma}(t)=\int_0^t \mathbf{C}(t-\tau):\frac{d\varepsilon(\tau)}{d\tau}d\tau, \tag{1}$$

where $\boldsymbol{\sigma}(t)$ is the stress tensor; $\varepsilon(t)$ is the strain tensor; $\mathbf{C}(t)$ is the relaxation tensor, which, unlike the tensor of elastic constants $\mathbf{C}$, describes the time dependence of the material response and takes into account the history of deformation.

As part of the study, it is assumed that the material is isotropic; therefore, $\mathbf{C}(t)$ can be decomposed into shear and bulk parts:

$$\mathbf{C}(t)=2G(t)\mathbf{I}_d+K(t)\mathbf{I}\otimes\mathbf{I}, \tag{2}$$

where $G(t)$ is shear modulus; $K(t)$ is modulus of volume compression; $\mathbf{I}_d$ is tensor of projection on the deviator part of the deformation; $\mathbf{I}\otimes\mathbf{I}$ is tensor of projection on the volume part of the deformation; $\otimes$ is tensor product.

Any positively defined relaxation function $G(t)$ and $K(t)$ can be represented as an integral over the relaxation spectrum:

$$S(t)=S_\infty+\int_0^t H(\tau)e^{-t/\tau}d\tau, \tag{3}$$

where S_∞ is the residual (final) modulus; $H(\tau)$ is the spectral density of relaxation. Such a decomposition $G(t)$ $K(t)$ corresponds to a continuous set of Maxwell elements (consecutive connection of the elastic and viscous elements).

To approximate the final sum of the integral, in modern computer-aided design systems, Prony series are widely used:

$$\int_0^t H(\tau)e^{-t/\tau}d\tau\approx\sum_{i=1}^{N}\alpha_i S_0 e^{-t/\beta_i}, \tag{4}$$

where $\alpha_i=\int_{\beta_{i-1}}^{\beta_i}H(\tau)d\tau\Big/S_0$ is the relative weight of the *i*-th element; β_i is the characteristic relaxation time on the *i*-th interval; N is the number of members of the series.

Based on (3) and (4), the shear modulus (5) and the volumetric compression modulus (6) have the form

$$G(t)=G_0\left[\alpha_\infty^G+\sum_{i=1}^{N_G}\alpha_i^G e^{-t/\beta_i^G}\right], \tag{5}$$

 doi:10.20944/preprints202605.1707.v1

$$K(t) = K_0\left[\alpha_\infty^K + \sum_{i=1}^{N_K} \alpha_i^K e^{-t/\beta_i^K}\right], \tag{6}$$

where α_∞ is the relative weight of the residual element.

The coefficients α_i are the relative weights of the relaxation spectrum elements and are dimensionless quantities. To ensure the physical consistency of the model, the normalization condition $\alpha_\infty + \sum_{i=1}^{N} \alpha_i = 1$ is met.

Based on the ratios (2)-(6), the connection with the stress (1) has the form:

$$\boldsymbol{\sigma}(t) = 2G_0 \int_0^t \left[\alpha_\infty^G + \sum_{i=1}^{N_G} \alpha_i^G e^{-t/\beta_i^G}\right] \frac{\mathbf{de}(\tau)}{d\tau} d\tau + \mathbf{I}K_0 \int_0^t \left[\alpha_\infty^K + \sum_{i=1}^{N_K} \alpha_i^K e^{-t/\beta_i^K}\right] \frac{d\theta(\tau)}{d\tau} d\tau, \tag{7}$$

where $\mathbf{e}(\tau)$ is the deviator of the strain tensor; $\theta(\tau)$ is the volumetric strain.

As part of the work, it is assumed that $K(t) = K_0 = \text{const}$. This assumption is typical for a wide class of polymeric materials, which is associated with insignificant effects of relaxation of volumetric deformations. Therefore, the ratio (7) takes the form:

$$\boldsymbol{\sigma}(t) = 2G_0 \int_0^t \left[\alpha_\infty^G + \sum_{i=1}^{N_G} \alpha_i^G e^{-t/\beta_i^G}\right] \frac{\mathbf{de}(\tau)}{d\tau} d\tau + \mathbf{I}K_0\theta, \tag{8}$$

DMA makes it possible to obtain the distribution of Young's modulus from the frequency and temperature. In a three-point bend, the modulus of elasticity is determined on the basis of the classical Euler-Bernoulli beam theory, in which the deformations are considered small, and the shear effects are negligible. Under these conditions, the bending stress-strain state is described by normal stresses associated with deformations through Young's modulus. Similarly to $G(t)$, we write the relaxation function for Young's modulus $E(t)$:

$$E(t) = E_0\left[c_\infty + \sum_{i=1}^{N_E} c_i e^{-t/\beta_i^E}\right], \tag{9}$$

where c_i is the relative weight of the *i-th* element; β_i^E is the characteristic relaxation time on the *i-th* interval for $E(t)$.

Assuming the correspondence of the characteristic relaxation times $E(t)$ and $G(t)$, the relationship of the relative weights of the functions (5) and (9) can be written as:

$$\sum_{i=1}^{N} \alpha_i = \sum_{i=1}^{N} c_i \left(E_0\left[G_0 - G_\infty\right] / \left(G_0\left[E_0 - E_\infty\right]\right)\right), \tag{10}$$

Knowing K_0, it is possible to determine the initial $G_0 = 3K_0E_0/(9K_0 - E_0)$ and final $G_\infty = 3K_\infty E_\infty/(9K_\infty - E_\infty)$ shear modulus. The modulus of volumetric compression is from the experimental data on Poisson's ratio $K_0 = E_0/(3(1-2\nu_0))$.

To take into account the temperature, the Williams-Landel-Ferry (WLF) temperature-time shift function is used:

$$A_{WLF}(T) = 10^{C_1(T-T_r)/(C_2+(T-T_r))}, \tag{11}$$

 doi:10.20944/preprints202605.1707.v1

where $A_{WLF}(T)$ is shear function; T_r is base temperature; C_1, C_2 are material parameters.

Within the framework of this approach, the characteristic relaxation time on the *i*-th interval is associated with (11) $\beta_i'(T)=\beta_i/A_{WLF}(T)$. Thus, the temperature effect on the behavior of the material is taken into account by changing the characteristic relaxation times, while the relative weights of the elements remain unchanged. This corresponds to the assumption of the thermological simplicity of the material. To describe the storage module (12) and the loss module (13) obtained using DMA, we will use the following relations:

$$E'(\omega;T)=E_0\left[c_\infty+\omega^2\sum_{i=1}^{N}c_i\frac{\beta_i'^2}{1+(\omega\beta_i')^2}\right], \tag{12}$$

$$E''(\omega;T)=E_0\,\omega\sum_{i=1}^{N}c_i\frac{\beta_i'}{1+(\omega\beta_i')^2}, \tag{13}$$

where $E'(\omega;T)$ is the storage module; $E''(\omega;T)$ is the loss module; ω is the frequency.

Thus, to describe the thermomechanical behavior of polymer materials, it is necessary to identify the parameters of the Prony series. The vector of unknowns has the form:

$$\bar{\mathbf{x}}=\left\{C_1;\,C_2;\,T_r;\,\alpha_i;\,\beta_i;\,i=\overline{1:N}\right\}, \tag{14}$$

2.4. Identification Procedure

The parameters of the viscoelastic model are determined based on experimental DMA data, in which frequency and temperature dependencies $E'(\omega;T)$ and $E''(\omega;T)$ are measured.

Identification of parameters is formulated as a problem of minimizing the deviation between experimental and calculated values. The root-mean-square error acts as a functional and has the form:

$$\Phi(\bar{\mathbf{x}})=\sum_{i=1}^{N_T}\left[\left(E'_{exp}(\omega;T_i)-E'_{num}(\omega;T_i;\bar{\mathbf{x}})\right)^2+\left(E''_{exp}(\omega;T_i)-E''_{num}(\omega;T_i;\bar{\mathbf{x}})\right)^2\right]\to\min \tag{15}$$

Minimization of the functionality $\Phi(\bar{\mathbf{x}})$ is carried out by the Nelder-Mead method by the gradientless optimization method. It is based on the sequential transformation of the simplex in the parameter space and does not require the calculation of derivatives of the objective function. This makes it effective for solving problems with a nonlinear parametric dependence of the material behavior model.

The physical limitations of the parameters are taken into account in the process of their identification:

$$C_1>0;\ C_2>0;\ \ \alpha_i>0,\ \beta_i>0,\ i=\overline{1:N};\ \sum_{i=1}^{N}\alpha_i=(G_0-G_\infty)/G_0\,. \tag{16}$$

The initial values of the relaxation times are set uniformly on a logarithmic scale, providing coverage of a wide range of characteristic times. The weighting factors are selected based on the normalization condition.

The optimization process is completed when the specified convergence criterion is reached—the error is less than 5%. As a result, the parameters of the Prony series and the temperature shift functions are determined and ensure the best matching of the model with the experimental DMA data.

2.4. Numerical Identification Procedure

 doi:10.20944/preprints202605.1707.v1

The numerical identification procedure uses the previously described defining ratios and a dataset of experimental studies. Figure 3 shows a diagram of its implementation.

The simplified scheme of the numerical procedure for identifying the material model contains three stages.

The first stage includes the initial processing of data from a series of computational experiments and the formation of a dataset. It includes data on the thermomechanics of materials and is used to evaluate the numerical model.

The second stage includes: the formation of finite element analysis modules, the choice of a material model, and the formation of defining relations, taking into account known theories and the general form of the vector of unknowns. The article considers a viscoelastic model of Maxwell's body. However, the possibilities of a numerical identification procedure are wider and include the construction of viscoelastic and elastic-visco-plastic models of materials. Simulation modeling of the DMA experiment is also included in the second stage. CAE modules are the results of the second stage and are used by the model parameter search algorithm.

The numerical algorithm of multiparameter optimization, the formation of the starting vector of unknowns, the management of the implementation of the solution of the problem using CAE software modules, and the automated processing of the results are implemented using Python. The vector of unknown models is specified iteratively. The numerical identification procedure is completed if the error between the numerical solution and the experimental dataset is less than 5%.

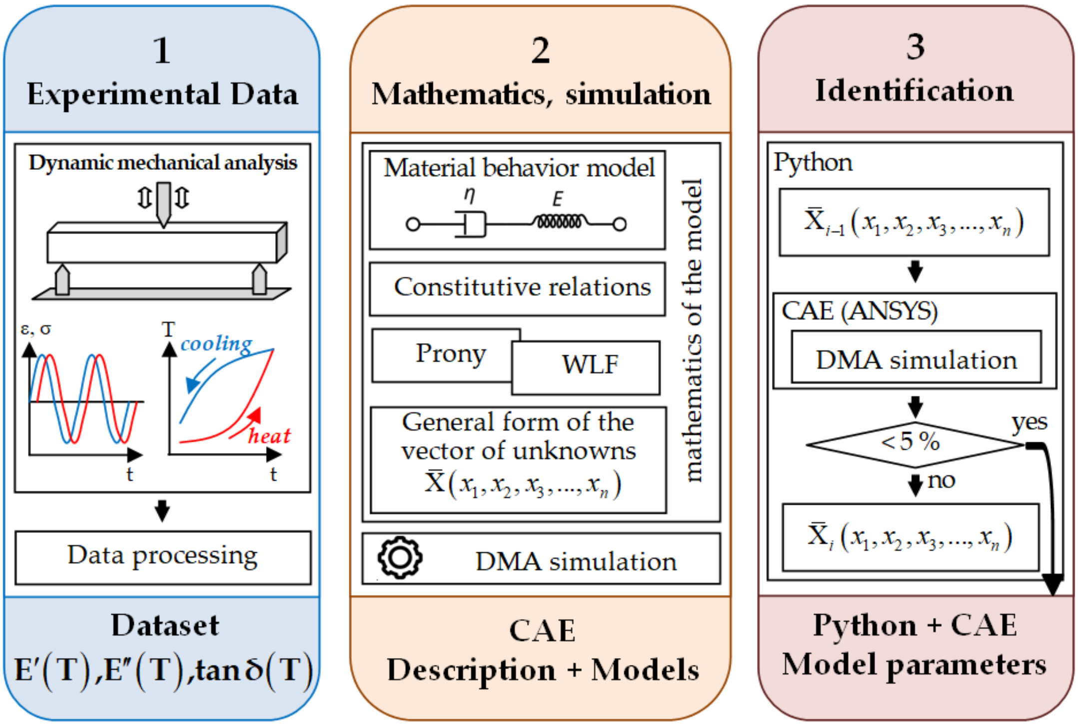

Figure 3. Diagram of a numerical procedure for identifying a mathematical model of the behavior of antifriction materials within the framework of viscoelasticity.

The final vector of the Maxwell model parameters based on Prony series and WLF parameters is formed as a result of the numerical identification procedure. The model is formed in the framework of the script for ANSYS.

2.5. Analysis of the Behavior of Antifriction Materials During Deformation of the Spherical Support Part, Taking into Account the Temperature Factor

 doi:10.20944/preprints202605.1707.v1

The work of antifriction materials is considered as part of the deformation of the spherical support part L-100 (AlfaTech LLC, Perm, Russia), taking into account the influence of ambient temperature. The computational scheme is presented in Figure 4.

The contact unit of the spherical support part represents two steel plates (1)-(2) separated by an antifriction polymer or composite layer (3). The minimum standard size of the support part designed for the standard vertical load of 1000 kN is considered. The geometric parameters of the structure are shown in Figure 4. The frictional contact is implemented with a previously unknown nature of the distribution of contact states (slippage, adhesion, slippage) $S_{cont_1} - S_{cont_3}$ at a constant friction coefficient [50]. Vertical movements are prohibited on S_2. Characteristic load uniformly distributed as pressure (~55 MPa) is applied to S_1. Bending S_1 is prohibited. The ambient temperature is considered in the range from −40 °C to + 80 °C.

The steel structural elements were modeled in the framework of the theory of elasticity with an elastic modulus of 2e11, a Poisson's ratio of 0.3, and the CTE of 11.7×10^{-6}. The friction coefficient is chosen to be a constant value of 0.04 and corresponds to the manufacturer's data of the bridge bearings for the steel-polymer contact. In the first approximation, the Poisson's ratio of the materials of the sliding layer is 0.466, and the CTE is 8×10^{-5}; these values are considered to be the same for the entire set of materials. CTE is selected based on PTFE behavior data. However, it may have a temperature dependence. This requires additional research.

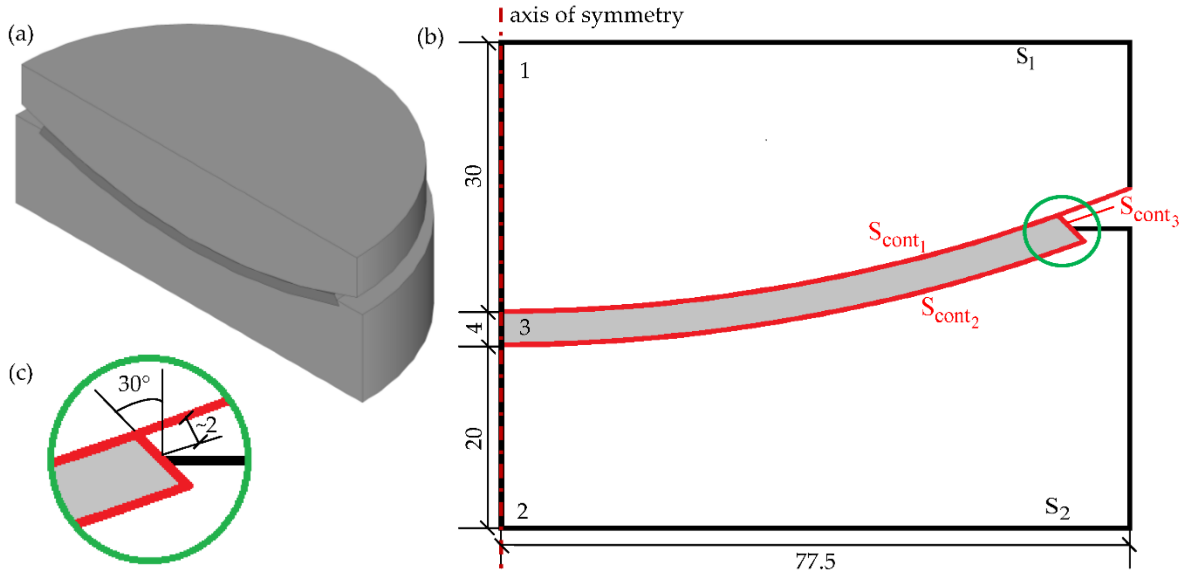

Figure 4. Spherical bridge bearing: a is the half contact unit (3D image); b is the computational scheme (central section, axisymmetric design); c is the end face of the sliding layer; 1 and 2 are top and bottom steel plates, correspondingly; 3 is the polymer/composite sliding layer; the green circle highlights the end face of the sliding layer.

The problem was implemented using the finite element method in ANSYS Mechanical APDL 2021R2 (Livermore, CA, USA). The model is considered in an axisymmetric formulation.

3. Results and Discussion

3.1. Experiment

The results of experiments are processed and evaluated relative to the standard deviation over the entire temperature range (Figure 5).

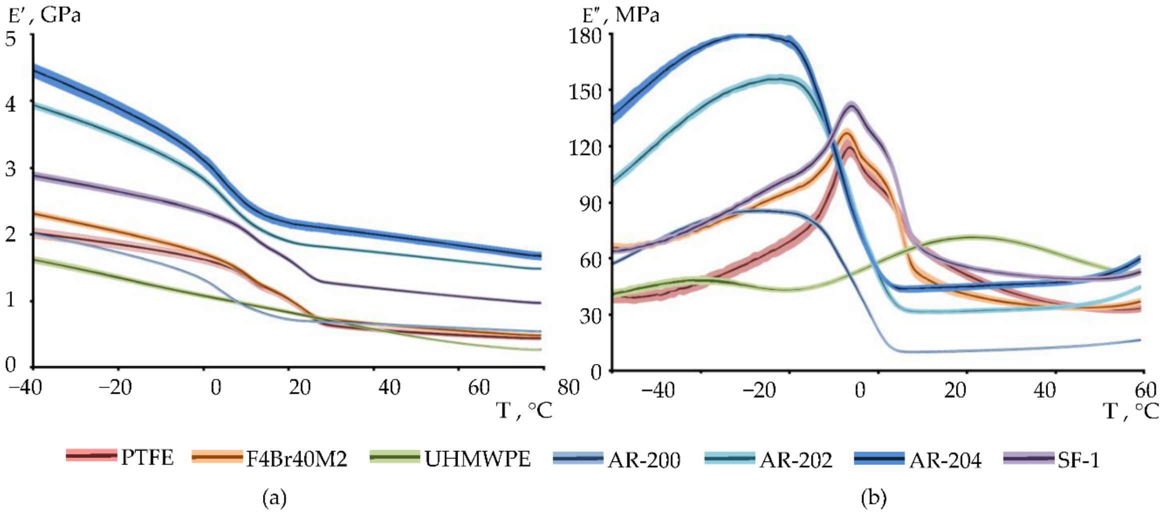

Figure 5. Dynamic mechanical analysis: a is the storage modulus; b is the loss modulus.

The maximum average deviation of the storage module is observed at a negative ambient temperature and decreases as the temperature rises. The maximum standard deviation of the storage module is observed in AR-204: at −40 °C – 101.36 MPa; at +80 °C – 54.53 MPa. The minimum standard deviation of the storage module is observed in AR-200: at −40 °C – 5.07 MPa; at +80 °C – 4.19 MPa. The standard deviation of the storage module of the remaining materials is in the range of 72.27-44.72 MPa at a temperature of −40 °C with a decrease to 23.03-6.56 MPa at +80 °C.

The standard deviation of the loss module has lower values compared to the standard deviation of the storage module. The nature of the change in the standard deviation of the loss module is similar to the storage module. The maximum values of the standard deviation of the loss module are fixed for PTFE: at −40 °C – 5.24 MPa; at +80 °C – 1.11 MPa. The minimum standard deviation of the loss module is observed for the material AR-200: at −40 °C – 1.61 MPa; at +80 °C – 0.09 MPa. For the remaining materials, the standard deviation of the loss module is 4.43-1.88 MPa at a temperature of −40 °C and decreases to 0.97–0.44 MPa at +80 °C.

The signal of the loss module makes it possible to determine the glass transition/softening temperature of the material [51]. The value of the temperature at which the maximum peak E'' is observed shows the glass transition temperature according to ASTME1640-18 “Standard test method for assignment of the glass transition temperature by dynamic mechanical analysis”. No apparent maximum E'' is observed in UHMWPE samples. This means that the glass transition temperature of UHMWPE does not fall within the temperature range in question. The glass transition temperatures of the remaining materials, obtained from the analysis of the temperature dependence $E''(T)$, are: +14 °C (288.15 K) is PTFE; +13 °C (287.15 K) is F4Br40M2; −6 °C (268.15 K) is AR-200; −2 °C (272.15 K) is AR-202; −9 °C (265.15 K) is AR-204; +14 °C (288.15 K) is SF-1.

The introduction of the nanofiller into the PTFE matrix leads to an increase in the storage modulus. The maximum effect is observed with modified PTFE filled with carbon fiber (AR-204). A similar trend is observed when carbon fiber is introduced as a nano-additive into polymer materials of a different nature and manufacturing technology [52]. The casting coke spiked material (AR-202) also has a significant increase in the storage modulus compared to pure PTFE. In materials AR-202 and AR-204, modified PTFE is used in the matrix composition. It is assumed that the combined effect of radiation exposure of the matrix and the nano-additive gives the maximum effect of increasing the thermomechanical parameter. This is confirmed by the fact that a separate modification of PTFE (AR-200) and the introduction of a carbon fiber nano-additive (SF-1) did not allow obtaining such an effect. The temperature dependence distribution of the storage module is generally similar for all materials.

The effect of PTFE modification on the behavior of materials can be assessed using the loss module. The inclusion of nano-additives in the PTFE matrix leads to an increase in the loss modulus compared to pure PTFE, but does not affect the temperature dependence of the parameter. Modification of PTFE leads to a change in the dependence $E''(T)$, a shift in the glass transition/softening temperature to the temperature range below 0 °C, and a change in the rate of relaxation transition of materials. The materials have a transition region from a vitrified to a highly elastic state near the glass transition temperature. High modulus of losses of composites and PTFE modifications at negative temperatures enhances viscoelasticity and provides greater energy dissipation [53]. At positive temperatures, this trend is observed only in SF-1, while the differences from pure PTFE do not exceed 30 MPa.

The behavior of UHMWPE is significantly different from the behavior of PTFE, its modifications, and compositions, and is considered one of its alternatives. This is largely due to the wide distribution of the material in the polymer market [54], as well as its use as a sliding layer [47,55]. Areas of relaxation transitions are not observed in the temperature range under consideration. The material exhibits a greater elastic response than PTFE at a temperature range of [−4; +30] °C. Two temperature zones are observed where the material exhibits higher viscosity compared to PTFE.

3.2. Thermo-Viscoelastic Model of the Behavior of an Antifriction Material

3.1.2. Numerical Analog of the Material

Prony series description parameters were obtained for each material. The total number of iterations did not exceed 3000 when identifying parameters, with an average calculation time of about 10 minutes.

Figure 4 shows an example of the convergence of the parameter identification algorithm for E' with different iterations (1, 100, 1000, 2000, and 3000) for PTFE material.

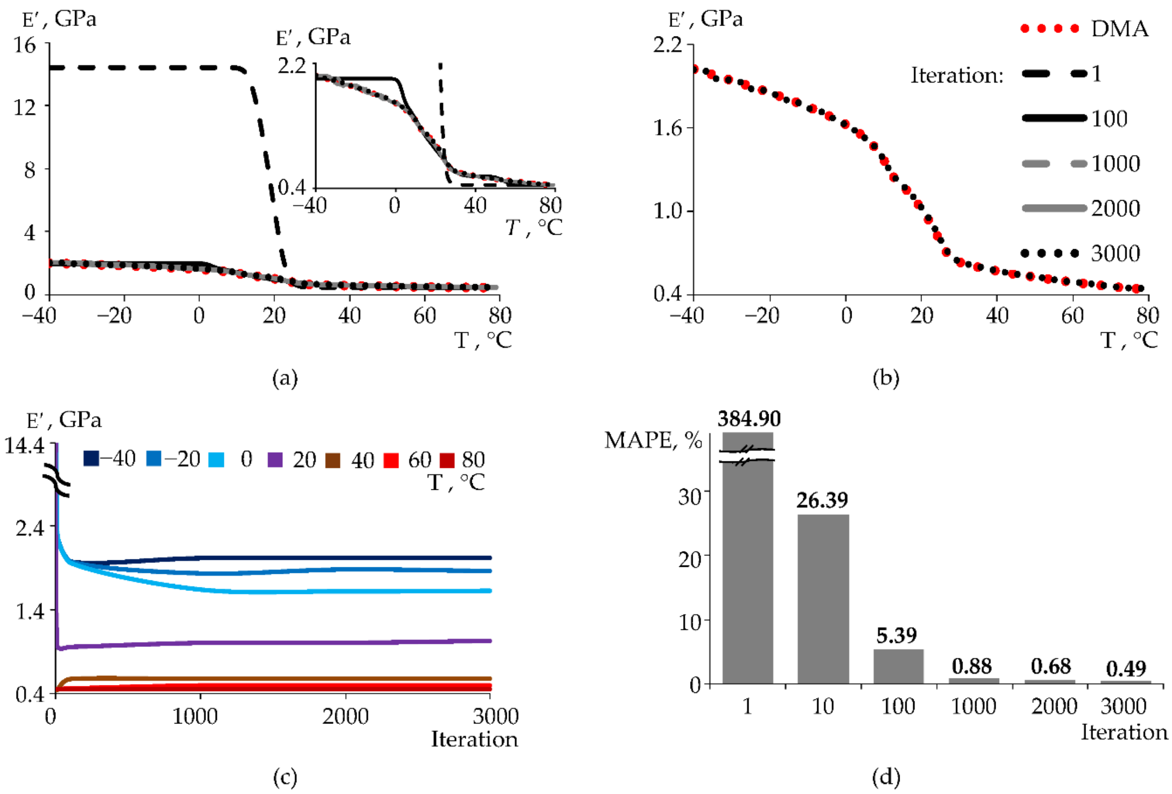

doi:10.20944/preprints202605.1707.v1

Figure 6. The convergence of the algorithm for identifying model parameters: a is convergence at different iterations; b is comparison of experimental data and solutions for the optimal vector of unknowns; c is dependence of the value of the storage modulus on iterations at different temperatures; d is mean absolute percentage error (MAPE).

The initial values of the parameters lead to a significant error between the experimental and calculated data (RMSE = 8.749). After 100 iterations, there is a satisfactory agreement of the results at temperatures below the glass transition temperature. The relative value of mean absolute percentage errors (MAPE) is on average not more than 6%, RMSE = 0.117.

The calculated values differ significantly from the experimental ones at temperatures above the glass transition temperature, which indicates a more complex nature of relaxation processes in this range.

The results obtained at 1000 and 2000 iterations demonstrate a marked improvement in approximation. However, the algorithm does not recognize them as the optimal solution. Fluctuations of E' are observed, although its values coincide well with the experimental data. The model parameters should provide a discrepancy between the numerical solution and the experiment of less than 5% over the entire data set. With an increase in the number of iterations to 3000, a good match of the model with the experimental data is achieved (MAPE = 0.49%, RMSE = 0.007). In this case, the solution is optimal. Deviations of numerical analogs from experimental data in the analysis of other materials have small differences from the deviations obtained for PTFE.

Based on the results of this procedure, parameters were obtained to describe the viscoelastic behavior of materials using Maxwell type equations (Tables 2–3), as well as WLF parameters (Table 2).

Table 2. The parameters of the Prony series and WLF.

Material	C_1	C_2	T_r, °K	E_0, MPa	E_∞, MPa
PTFE	203.908	849.003	270.214	2021.386	446.325
F4Br40M2	299.100	1069.367	263.790	2313.682	489.782
UHMWPE	288.378	1393.953	274.120	1624.766	280.550
AR-200	103.243	419.182	266.802	2006.566	541.677
AR-202	128.304	438.184	260.565	3945.537	1486.422
AR-204	51.796	175.616	253.551	4467.330	1675.070
SF-1	191.149	781.408	267.538	2882.213	974.841

Table 3. The 40 $\alpha_i - \beta_i$ pairs.

i	β_i	PTFE	F4Br40M2	UHMWPE	AR-200	AR-202	AR-204	SF-1
		α_i	α_i	α_i	α_i	α_i	α_i	α_i
1	1.00×10^{-9}	3.04×10^{-2}	2.42×10^{-2}	3.08×10^{-2}	2.90×10^{-2}	1.12×10^{-2}	5.13×10^{-3}	2.39×10^{-2}
2	5.54×10^{-9}	2.54×10^{-6}	1.12×10^{-2}	3.14×10^{-2}	1.28×10^{-2}	1.33×10^{-2}	1.15×10^{-3}	1.49×10^{-8}
3	3.07×10^{-8}	2.14×10^{-2}	1.22×10^{-2}	2.41×10^{-2}	2.13×10^{-2}	1.08×10^{-2}	2.40×10^{-4}	1.48×10^{-2}
4	1.70×10^{-7}	1.40×10^{-2}	1.83×10^{-2}	2.68×10^{-2}	2.57×10^{-2}	1.39×10^{-2}	1.24×10^{-2}	8.64×10^{-3}
5	9.43×10^{-7}	4.73×10^{-9}	1.23×10^{-2}	3.26×10^{-2}	5.22×10^{-5}	2.03×10^{-2}	3.01×10^{-3}	1.53×10^{-2}
6	5.22×10^{-6}	2.17×10^{-2}	1.70×10^{-2}	3.86×10^{-2}	4.47×10^{-2}	5.17×10^{-9}	2.50×10^{-2}	1.00×10^{-2}
7	2.89×10^{-5}	1.76×10^{-2}	2.28×10^{-2}	2.58×10^{-2}	4.84×10^{-3}	2.78×10^{-2}	2.49×10^{-2}	2.12×10^{-2}
8	1.60×10^{-4}	1.85×10^{-2}	2.93×10^{-12}	3.68×10^{-2}	3.17×10^{-2}	8.19×10^{-3}	1.33×10^{-3}	1.11×10^{-5}
9	8.89×10^{-4}	2.38×10^{-8}	2.94×10^{-2}	2.55×10^{-2}	2.17×10^{-2}	1.80×10^{-2}	1.48×10^{-2}	2.10×10^{-2}
10	4.92×10^{-3}	2.02×10^{-2}	2.35×10^{-2}	2.16×10^{-2}	2.34×10^{-2}	1.98×10^{-2}	4.86×10^{-3}	2.13×10^{-2}
11	2.73×10^{-2}	1.83×10^{-2}	7.84×10^{-9}	3.75×10^{-2}	4.75×10^{-2}	1.33×10^{-2}	3.10×10^{-2}	7.11×10^{-12}
12	1.51×10^{-1}	2.83×10^{-2}	2.57×10^{-2}	2.53×10^{-2}	3.14×10^{-5}	2.11×10^{-2}	1.59×10^{-2}	3.78×10^{-2}
13	8.38×10^{-1}	1.83×10^{-2}	2.69×10^{-2}	2.73×10^{-2}	6.33×10^{-2}	2.23×10^{-2}	2.34×10^{-2}	3.00×10^{-10}
14	4.64×10^{0}	2.85×10^{-2}	1.40×10^{-2}	3.15×10^{-2}	2.66×10^{-2}	1.38×10^{-2}	2.02×10^{-2}	4.46×10^{-2}

Preprints.org (www.preprints.org) | NOT PEER-REVIEWED | Posted: 26 May 2026 doi:10.20944/preprints202605.1707.v1

15	2.57×10^{1}	3.66×10^{-2}	2.32×10^{-2}	2.11×10^{-2}	1.06×10^{-1}	4.59×10^{-2}	1.83×10^{-2}	1.10×10^{-7}
16	1.43×10^{2}	9.30×10^{-2}	2.34×10^{-2}	2.05×10^{-2}	3.88×10^{-2}	2.39×10^{-15}	1.94×10^{-2}	5.58×10^{-2}
17	7.90×10^{2}	3.94×10^{-2}	5.56×10^{-2}	4.37×10^{-2}	7.59×10^{-2}	5.49×10^{-2}	2.69×10^{-2}	4.15×10^{-2}
18	4.38×10^{3}	5.13×10^{-2}	1.12×10^{-15}	4.63×10^{-2}	2.91×10^{-2}	3.80×10^{-2}	4.77×10^{-2}	4.73×10^{-2}
19	2.42×10^{4}	5.72×10^{-2}	8.37×10^{-2}	3.79×10^{-5}	3.20×10^{-2}	5.11×10^{-2}	3.86×10^{-2}	6.10×10^{-2}
20	1.34×10^{5}	8.20×10^{-2}	4.10×10^{-2}	2.59×10^{-2}	1.38×10^{-2}	4.13×10^{-2}	3.51×10^{-2}	2.63×10^{-2}
21	7.44×10^{5}	8.56×10^{-2}	4.19×10^{-2}	6.33×10^{-2}	1.58×10^{-2}	3.36×10^{-2}	6.18×10^{-2}	7.91×10^{-2}
22	4.12×10^{6}	1.24×10^{-2}	3.40×10^{-2}	6.45×10^{-6}	3.35×10^{-3}	2.26×10^{-2}	4.38×10^{-2}	2.42×10^{-2}
23	2.29×10^{7}	1.20×10^{-2}	5.52×10^{-2}	3.32×10^{-2}	2.99×10^{-3}	1.86×10^{-2}	2.22×10^{-2}	1.51×10^{-2}
24	1.27×10^{8}	1.22×10^{-2}	5.91×10^{-2}	3.20×10^{-2}	4.13×10^{-3}	1.99×10^{-2}	2.93×10^{-2}	1.70×10^{-2}
25	7.02×10^{8}	6.11×10^{-10}	3.79×10^{-2}	2.66×10^{-2}	8.45×10^{-5}	1.94×10^{-13}	3.48×10^{-3}	3.64×10^{-6}
26	3.89×10^{9}	1.66×10^{-2}	2.40×10^{-15}	1.51×10^{-2}	1.01×10^{-2}	5.37×10^{-3}	5.87×10^{-3}	1.48×10^{-2}
27	2.15×10^{10}	4.07×10^{-3}	1.59×10^{-2}	2.56×10^{-2}	8.59×10^{-3}	1.51×10^{-2}	3.32×10^{-3}	6.91×10^{-8}
28	1.19×10^{11}	5.14×10^{-5}	1.53×10^{-3}	2.83×10^{-2}	$7.32\times10-5$	3.60×10^{-14}	1.15×10^{-2}	4.65×10^{-3}
29	6.61×10^{11}	1.97×10^{-2}	5.44×10^{-3}	1.21×10^{-2}	1.24×10^{-2}	4.69×10^{-11}	3.35×10^{-3}	1.79×10^{-2}
30	3.67×10^{12}	1.48×10^{-6}	1.62×10^{-2}	1.13×10^{-2}	7.92×10^{-3}	1.17×10^{-11}	1.30×10^{-2}	1.11×10^{-9}
31	2.03×10^{13}	1.33×10^{-2}	5.48×10^{-8}	2.79×10^{-3}	1.44×10^{-3}	1.64×10^{-2}	1.51×10^{-2}	1.04×10^{-2}
32	1.13×10^{14}	5.21×10^{-7}	1.30×10^{-2}	1.20×10^{-3}	6.84×10^{-3}	5.19×10^{-3}	3.81×10^{-4}	1.27×10^{-2}
33	6.24×10^{14}	1.45×10^{-4}	1.43×10^{-12}	8.18×10^{-3}	5.81×10^{-3}	4.54×10^{-14}	9.57×10^{-3}	1.41×10^{-5}
34	3.46×10^{15}	9.02×10^{-8}	8.15×10^{-3}	8.18×10^{-8}	4.67×10^{-3}	1.10×10^{-2}	2.14×10^{-2}	1.04×10^{-2}
35	1.91×10^{16}	1.34×10^{-2}	1.39×10^{-2}	3.60×10^{-5}	4.83×10^{-3}	2.81×10^{-3}	7.93×10^{-3}	1.18×10^{-2}
36	1.06×10^{17}	4.61×10^{-10}	3.09×10^{-10}	5.97×10^{-6}	1.75×10^{-5}	1.08×10^{-2}	6.62×10^{-3}	1.84×10^{-4}
37	5.88×10^{17}	1.27×10^{-7}	7.26×10^{-4}	1.44×10^{-8}	7.90×10^{-7}	3.15×10^{-21}	2.79×10^{-3}	3.15×10^{-7}
38	3.26×10^{18}	4.15×10^{-8}	1.28×10^{-2}	3.33×10^{-6}	2.23×10^{-4}	1.11×10^{-2}	2.17×10^{-3}	7.70×10^{-11}
39	1.80×10^{19}	6.61×10^{-7}	6.24×10^{-16}	6.18×10^{-9}	1.67×10^{-4}	1.13×10^{-3}	3.95×10^{-4}	2.22×10^{-3}
40	1.00×10^{20}	8.50×10^{-12}	1.48×10^{-2}	1.82×10^{-4}	2.40×10^{-8}	1.41×10^{-2}	1.04×10^{-3}	2.93×10^{-5}

In the first approximation, one set of parameters is used to describe the behavior of materials in a temperature range from −40 °C to +80 °C. However, in almost all materials (except UHMWPE), the glass transition/softening temperature falls into the considered temperature range. There is a hypothesis that it is necessary to take into account the differences in the behavior of materials before and after reaching the glass transition temperature [56,57]. Temperature has a strong impact on the behavior of polymer and composite materials [58]. The glass transition temperature is one of the key factors determining the viscoelastic behavior of polymer materials [59]. The main limitation of the current model of thermomechanics of antifriction materials is one set of parameters to describe their behavior over the entire temperature range of operation. The direction of future research is the expansion of the identification procedure and modification of the algorithm for modeling the behavior of materials, taking into account the difference in the nature of their mechanical response at temperatures below and above the glass transition temperature.

3.2.2. Analysis of the Influence of Finite-Element Partitioning on the Numerical Solution of the Problem

The first stage of the numerical study included an assessment of the effect of the finite element (FE) mesh on the numerical solution of the problem. Repeatability was investigated at an ambient temperature of +20 °C. The material of the sliding layer was PTFE. Earlier studies found the presence of fluctuations S_{cont_1} due to the lack of complete coincidence of the nodes of the mesh of CONTA-TARGE elements. TARGE S_{cont_1} and CONTA S_{cont_2} were separated in such a way as to ensure the maximum overlap at initial contact. The formation of the FE mesh on the interface surfaces of elements has a strong impact on the solution of contact problems, despite the development of computing packages, methods, approaches, and algorithms [60,61]. Conformal models require the formation of a node-to-node mesh to eliminate the constraints of solving the problem.

 doi:10.20944/preprints202605.1707.v1

Three variants of the FE mesh were considered: 1 is a uniform mesh with the same overall size of elements in all volumes of the model; 2 is a mesh in which the overall size in steel elements is twice as large as in the sliding layer; 3 is a mesh with a uniform partition in the volume of the sliding layer and a gradient increase in the size of the element in steel plates from the contact area (the maximum size of the elements was doubled to the surfaces remote from the contact zone). All meshes are implemented using quadrilateral elements with Lagrangian approximation. Figure 7 shows the view of FE meshes for the sliding layer with the overall size of the elements of 0.5 mm.

(a)

(b)

(c)

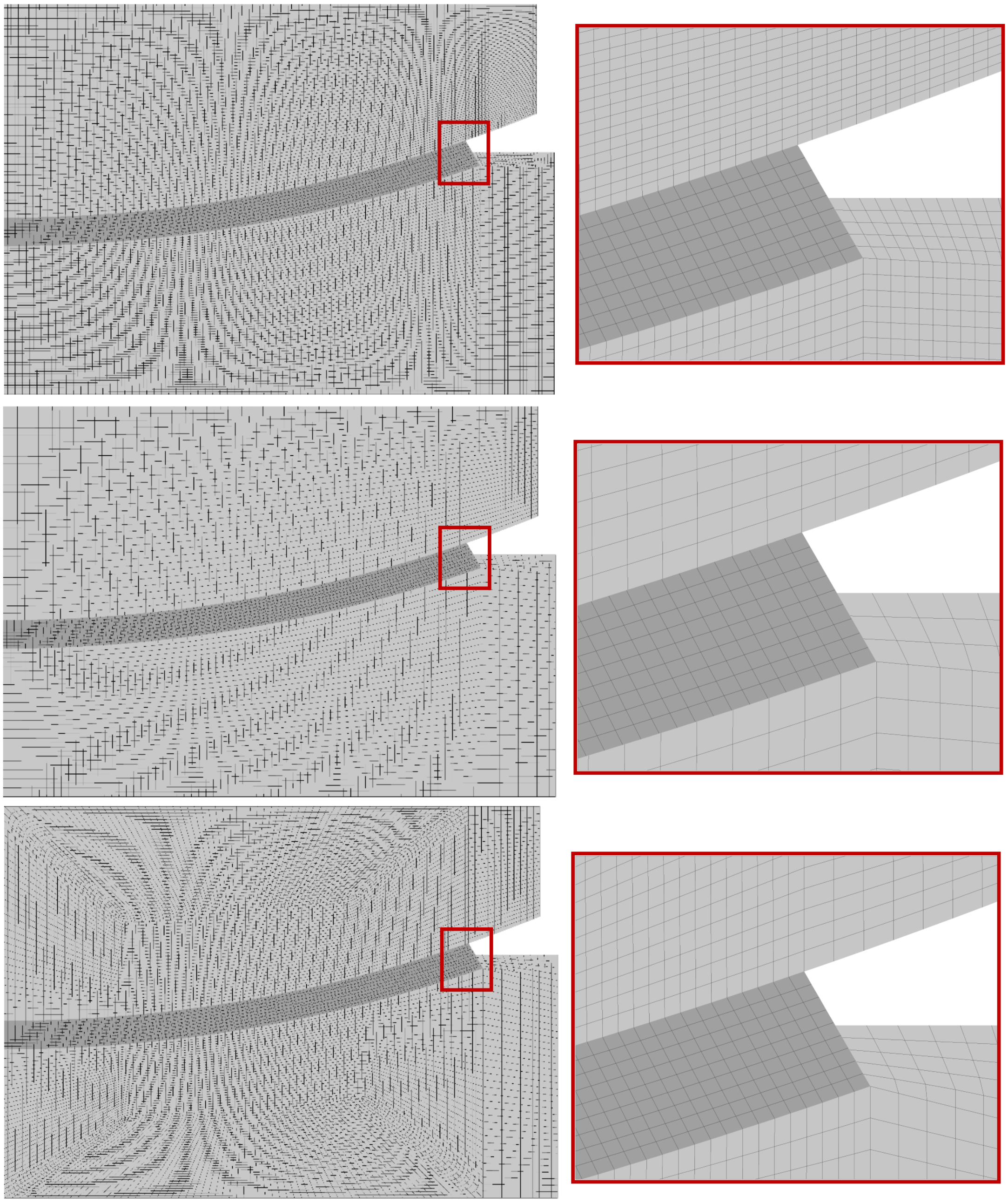

Figure 7. Finite element partition: a is mesh 1; b is mesh 2; c is mesh 3.

Two types of finite elements are considered for constructing the FE mesh: 1 is first-order elements (PLANE182, CONTA171, TARGE169); 2 is second-order elements (PLANE183, CONTA172, TARGE169). Higher-order elements have been considered in connection with their effectiveness for modeling nonlinear contact, especially in the nonlinear behavior of materials [62].

Past studies have established the need for high-quality construction of an FE mesh in the area of mating of steel elements and a sliding layer [63]. The minimum overall dimension of the element is related to the thickness of the sliding layer. Table 4 presents the FE mesh parameters.

Table 4. The parameters of the finite element mesh.

Number of elements by sliding layer thickness (N)	**4**	**8**	**12**	**16**	**24**	**32**	**40**
Minimum overall dimension of the element, mm	1.000	0.500	0.330	0.250	0.167	0.125	0.100

The article investigated the convergence of the numerical solution through the example of maximum vertical displacements (Figure 8).

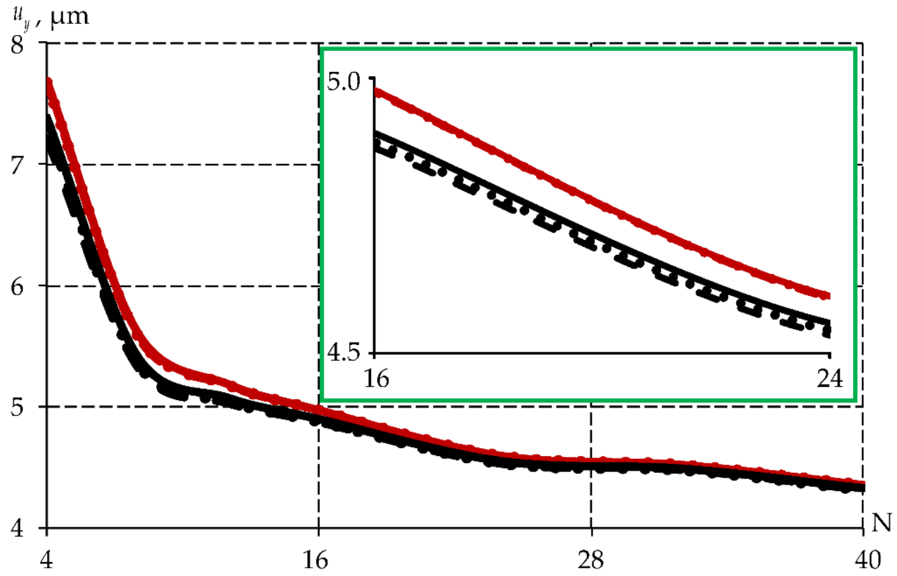

Figure 8. The convergence of the numerical solution of the problem by the example of vertical displacements: black is elements of the first order; red is elements of the second order; the solid line is mesh 1; the stroke is mesh 2; points are mesh 3.

The change in the values of the vertical displacement of the support part does not exceed 8% for all types of mesh elements, when dividing the sliding layer into 16 and 24 elements. Further refinement of the mesh leads to a change in the parameter by no more than 1.2–3.6%. It can be noted that the value of the parameter is higher when using two order elements. However, the differences do not exceed 5% in the case of meshes 1 and 3 and 6.3% in the case of mesh 2. The difference in the vertical displacements of the model does not exceed 2% when using elements of the 1st and 2nd order with a mesh with 16 elements along the thickness of the layer.

For all mesh configurations, the maximum values of stress intensity and contact pressure differ by less than 1% for meshes with division into 16 and 24 elements by the thickness of the sliding layer.

Differences in solutions with different meshes with first-order elements do not exceed 2.5%, with second-order elements less than 0.6%. However, when using first-order elements in mesh 2, fluctuations S_{cont_1} are observed—local variations in the contact pressure in adjacent elements in the range of about 2 MPa.

The time for solving the problem within the framework of static loading is several seconds when using first-order elements with a gradient increase in the element from the interface area. Mesh 2 converges more slowly than the other two FE meshes. The use of higher-order elements also increases the calculation time, and their use is not always justified and effective. At the same time, elements with linear functions of the shape make it possible to obtain a high-quality solution with qualitatively constructed meshes and properly developed algorithms [64,65].

As a rational mesh, a mesh was chosen using first-order elements, containing 16 elements in the thickness of the interlayer and a gradient increase in the elements in the steel plates as the distance from the contact surfaces with the sliding layer. The discretization of the system is approximately 116 thousand nodal unknowns in such a partition. It provides the required accuracy of the solution without increasing the load of computing power. This will be relevant when moving to the analysis of the influence of the time factor and the frequency of loading, which are planned in future studies.

3.3.3. Thermomechanical Deformation of the Spherical Support Part of the Bridge

The influence of temperature on the behavior of the materials of the sliding layer under the deformation of the spherical support part under the influence of the nominal load is analyzed. Figure 9 shows, by way of example, the distribution of contact parameters at an ambient temperature of +20 °C. The contact parameters are shown for S_{cont_1}, along which it is possible to rotate the spherical segment.

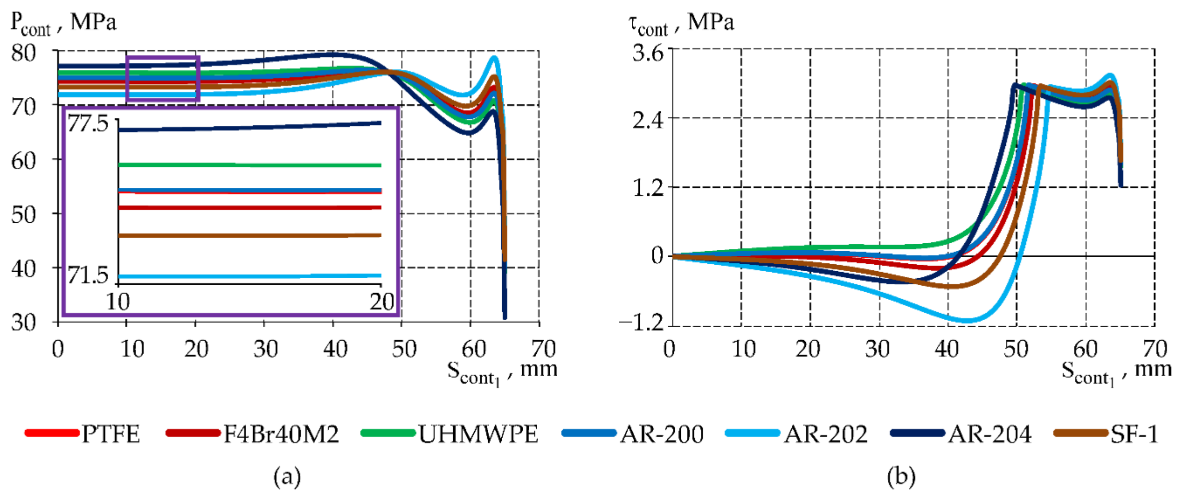

Figure 9. Contact parameters S_{cont_1} : a is the contact pressure; b is the contact shear stress.

The nature of the distribution of the contact pressure and the contact shear stress at S_{cont_1} does not depend on the material of the sliding layer. Divergence of the contact surfaces near the edge of the sliding layer is not observed for this temperature.

Modification of PTFE has no significant effect on the contact characteristics. The contact parameters of PTFE and AR-200 have small differences: contact pressure is less than 1%; contact shear stress is no more than 3% (on the main contact area). The differences can reach 36% near the zone of change of contact states from slip to adhesion.

The stick zone under full stick conditions is observed in the central part of the sliding surface. The maximum surface area in the adhesion state is observed in a structure with a layer of AR-202 (58.63% of the total contact area). Minimum—in a structure with a UHMWPE interlayer (47.41%). The boundary of the stick zone under full stick conditions can be determined by changing the contact parameters. The contact pressure varies slightly in the adhesion area (central zone of the support part). The zone in which the contact shear stress reaches the plateau (stabilizes) corresponds to the transition from adhesion to slippage. The radius of the area of full adhesion of the interface surfaces S_{cont_1} varies from 49.39 to 54.55 mm.

The maximum level of contact pressure values during viscoelastic setting is offset relative to the center of the support part. It is observed mainly near the boundary of the transition of the contact state from adhesion to slippage. The maximum level of contact parameters is observed near the edge of the sliding layer of AR-202. Thus, for the contact pressure, it reaches 9.34% compared to the central part of the structure. The minimum increase in contact pressure relative to the central part (1.04%) is noted in a structure with a UHMWPE layer.

Basically, the maximum level of contact parameters of modern materials is commensurate with the interlayer of pure PTFE. In the comparative analysis with pure PTFE, the maximum differences in contact pressure were recorded for the layers of AR-202 (2.8%) and AR-204 (3.7%), while the maximum difference in contact shear stress (6.04%) was observed for the layer of AR-202. The contact pressure in the center of the supporting part of the structure with a layer of AR-202 is 4.17% less, and that of AR-204 is 2.88% more than in the structure with a PTFE interlayer. The difference of the remaining materials from the PTFE interlayer in contact parameters is less than 1%.

The absolute values of the contact parameters at S_{cont_2} have small differences from S_{cont_1}. The nature of the distribution of the contact pressure is more uniform, which is associated with the limited freedom of the interface. The nature of the distribution of the contact shear stress is opposite.

The maximum level of contact parameters is observed at S_{cont_3} (Figure 10). This is largely due to the relative freedom of the end of the sliding layer S_{cont_3}, as well as the presence of a stress concentrator in the area of the steel collar of the bottom plate of the support part.

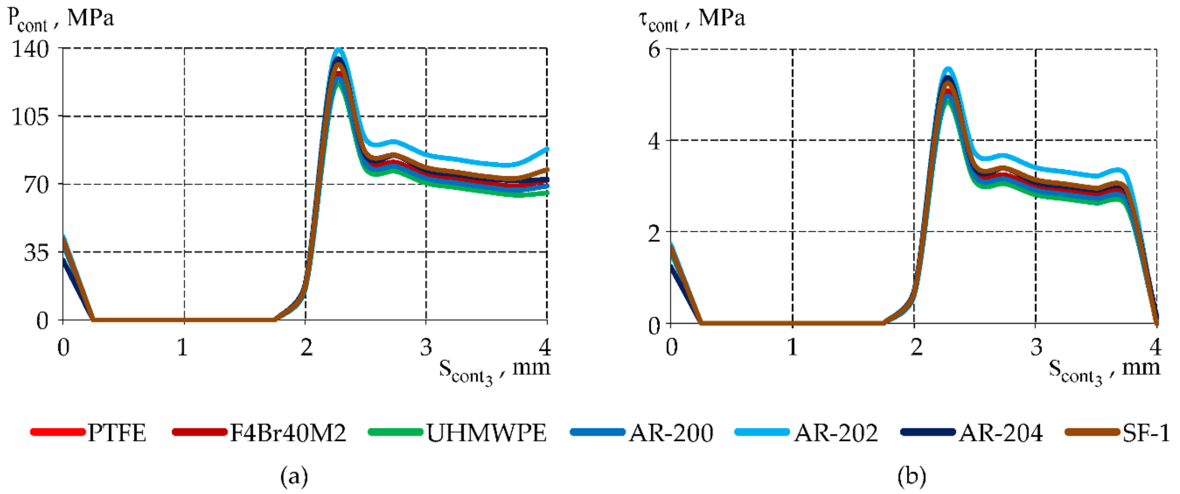

Figure 10. Contact parameters S_{cont_3} : a is the contact pressure; b is the contact shear stress.

The maximum level of contact parameters is observed near the edge of the mating of the end of the sliding layer with the lower steel plate. The maximum contact pressure level is on average 64.85% higher compared to $S_{cont_1} - S_{cont_2}$. The maximum level of the contact shear stress is on average 69.54% higher. The minimum values of the parameters are observed in a structure with a layer of UHMWPE, the maximum values are AR-202. All PTFE composites have a higher level of contact parameters than a pure PTFE interlayer at S_{cont_3}.

The displacements along the normal of the end of the sliding layer are one of the indicators of the material's work as part of the deformation of the spherical support part (Figure 11).

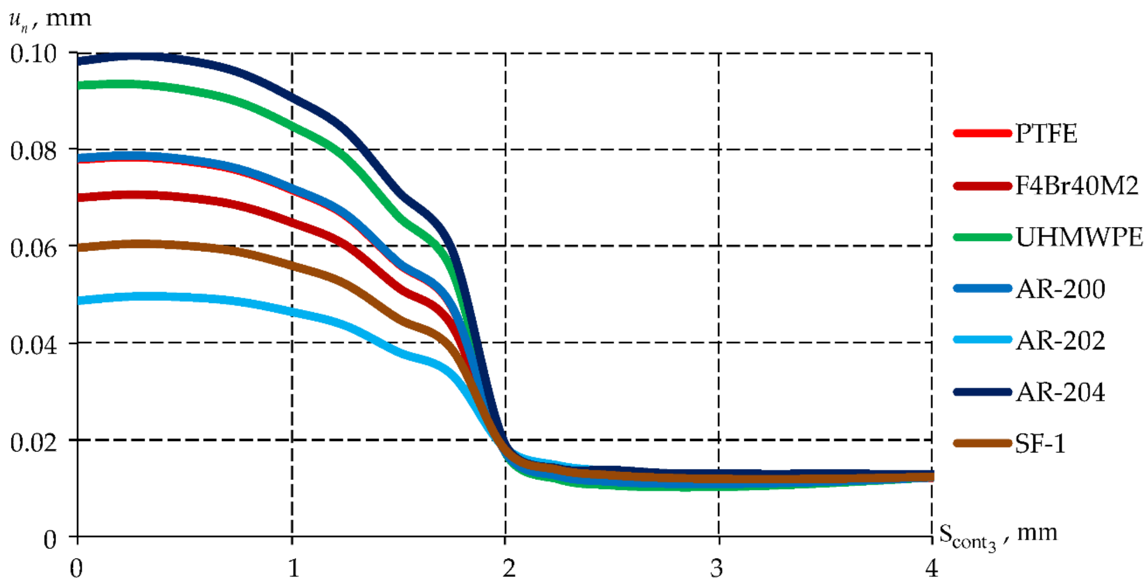

Figure 11. Movements along the normal of the end of the sliding layer.

The maximum normal displacements of the end of the sliding layer do not exceed 0.1 mm and are observed in the AR-204 layer. The minimum normal displacements are observed in the layer of AR-202 and reach 0.049 mm. The maximum normal displacements of the sliding layers of composite materials F4Br40M2 and SF-1 (0.07 and 0.06 mm, respectively) are less than that of a pure PTFE interlayer.

Temperature dependencies are obtained for the parameters of the contact and the stress-strain state of the sliding layer. The temperature dependencies of the maximum values of the parameters are well described by polynomial regression. The polynomial of the second degree well describes the behavior of the volume of the sliding layer and the main contact surfaces $S_{cont_1} - S_{cont_2}$. The dependence of the contact parameters of the end of the sliding layer is described by linear regression. The temperature dependencies of the main contact parameters of the stress-strain state are presented in Appendix A.

Figure 11 shows the temperature dependencies of the maximum intensity of stresses and deformations.

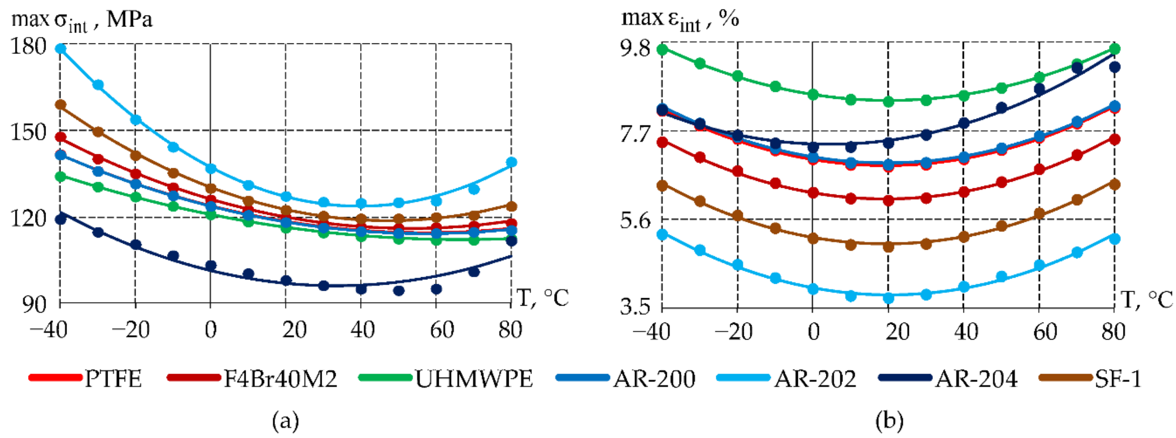

Figure 12. The temperature dependence of the maximum level of the stress-strain state parameters: a is the contact pressure; b is the contact shear stress; the marker is the numerical data; the line is the approximation.

The maximum stress intensity is more sensitive to ambient temperature. The value of the parameter is higher at negative temperatures.

The maximum stress intensity on average is described with a coefficient of determination R^2 of 0.9856 and an average error size RMSE of 0.1848. Approximately 50% of the volume of the sliding layer experiences hydrostatic compression due to the presence of a full adhesion zone in the contact. The maximum stress intensity is observed near the stress concentrator of the end of the sliding layer. This applies to the structural features of the support part and does not depend on the material model [66,67]. The material model and external factors, including temperature, affect the maximum values of the parameter and the volume of the layer in which the maximum is observed. The location of the maximum stresses of the spherical sliding layer is correlated with the data of Wei et al. [68].

The maximum stress intensity in the volume of the sliding layer of F4Br40M2; UHMWPE differs from PTFE on average by no more than 3%. In a structure with a layer of SF-1, this figure is on average 6% higher. The maximum differences in stress intensity are observed in the layers of AR-202 and AR-204. The stress intensity of the AR-202 layer is on average 13% higher. The opposite effect is observed in the AR-204 layer, where the stress intensity is on average 15% less. The minimum differences in stress intensity compared to pure PTFE are observed in the AR-200 layer and reach a maximum of 0.13%.

The maximum intensity of deformations has a greater spread between the materials of the sliding layer. The average coefficient of determination R^2 of the mathematical description of the temperature dependence of the maximum strain intensity is 0.99 at RMSE 0.0131. The maximum intensity of deformations of the sliding layer does not exceed 10%.

A comparative analysis of the maximum intensity of deformations in a layer of polymer/composite materials with a PTFE layer was carried out. For AR-202, the parameter values are on average 41% less. For UHMWPE, the maximum strain intensity is on average 20% higher. Minimal differences in the parameter are observed in AR-200 (less than 0.65%).

Figure 13 shows the temperature dependence of the maximum contact parameters on the main interface S_{cont_1}.

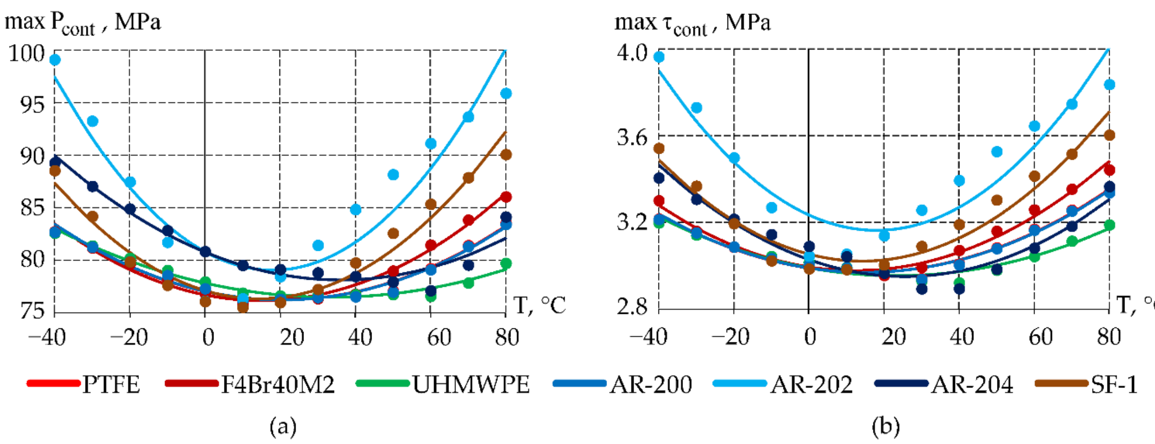

Figure 13. The temperature dependence of the maximum level of the contact parameters S_{cont_1} on T: a is the contact pressure; b is the contact shear stress; the marker is the numerical data; the line is the approximation.

The minimum values of the contact parameters are observed at a temperature range of [0; +20] °C. A comparable level of contact parameters is observed at maximum negative and positive temperatures. AR-202 has a maximum value of contact parameters and is more sensitive to ambient temperature compared to other materials. A higher-order polynomial can better describe the temperature dependence of contact parameters for the AR-200. The second-order polynomial describes the contact pressure with the lowest coefficient of determination $R^2 = 0.8732$ with the highest value of RMSE = 0.7199.

 doi:10.20944/preprints202605.1707.v1

The material of the sliding layer significantly affects the contact parameters. The maximum deviations relative to the PTFE interlayer are observed for AR-202: the contact pressure is on average 9.67% higher, and the contact shear stress is 11.88% higher. For UHMWPE, the deviation of the maximum contact pressure is on average 0.67% less, and the contact shear stress is 1.47% less. The use of other materials within the sliding layer leads to a slight increase in contact parameters, on average by no more than 4%.

Physical determination of the level of contact parameters is a difficult task. This is largely due to the geometric configuration of the structure. Therefore, numerical modeling is common to determine the contact parameters [69,70]. Recently, however, there has been a tendency to create intelligent bearings with the introduction of sensors into the design [71–73]. While this type of monitoring is not aimed at determining the contact characteristics of the system, it can be assumed that the further digitalization of the bearing construction industry over time will make it possible to determine the contact parameters when monitoring the state of the structure.

Figure 14 represents the temperature dependence of the maximum normal movements of the end of the sliding layer.

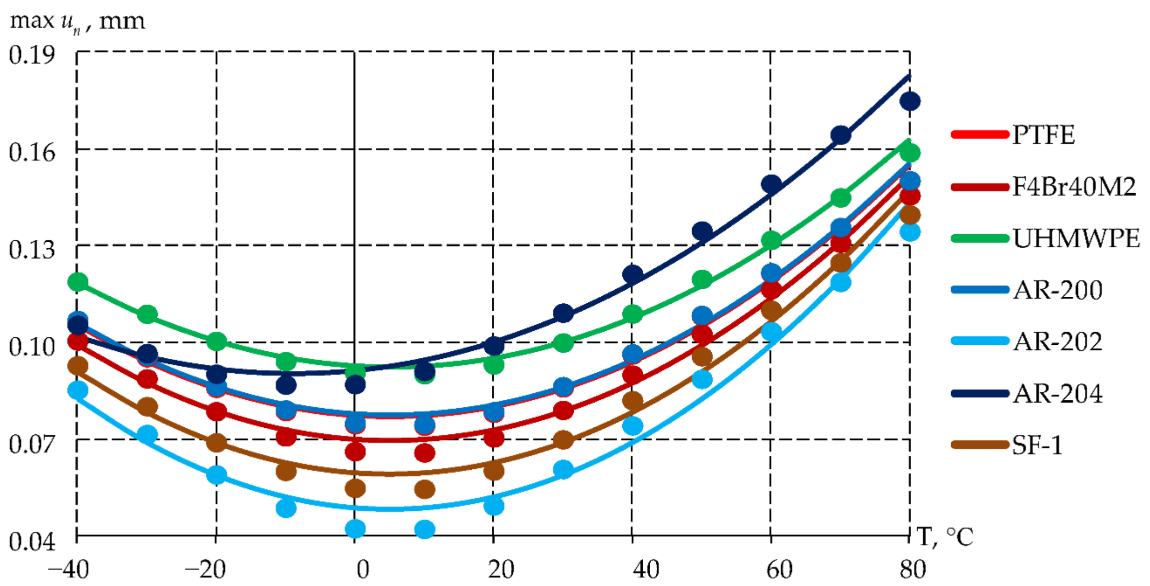

Figure 14. The temperature dependence of the maximum normal movements of the slip layer end: the marker is the numerical data; the line is the approximation.

The maximum normal displacements of the end of the sliding layer do not exceed 0.2 mm and are observed at an ambient temperature of +80 °C. For AR-202, this parameter is lower by an average of 26% compared to PTFE. A similar comparison shows that for AR-204, on average, normal displacements are 16.9% greater.

The level of displacements of the spherical bearing is commensurate with the results of experimental studies presented by Chen et al. [74].

Spherical bridge bearings are among the three most common configurations used for the mobility of the bridge span and damping loads from external influences [75]. Common defects of spherical bearings of bridges are destruction, strong deformation of Teflon layers of sliding, as well as degradation of the material. This confirms the need to assess the suitability of modern materials with improved physical and mechanical properties for use in antifriction sliding layers. Masi et al. emphasize the need to form a database on the reaction of materials to different types of load and temperature. Other authors [76,77] also emphasize the importance of assessing the effect of temperature effects on the operation of bridge bearings. Thus, temperature accounting is necessary to describe the behavior of non-metallic bearing materials. Within the framework of the current study, this is realized by constructing thermo-viscoelastic models of the behavior of the materials used or suitable for the sliding layers. This approach makes it possible to assess the behavior of the structure, taking into account the temperature and inelastic effects, which is important for the rationalization of its work [78].

5. Conclusions

The thermomechanics of a set of modern nanomodified polymers and composites suitable for use as sliding layers of friction units have been studied. Temperature dependencies of viscoelastic characteristics of materials have been determined at an ambient temperature of −40 to +80 °C. Numerical analogs of materials have been constructed according to experimental data (MAPE < 0.5%, RMSE < 0.01).

The behavior of these materials as a sliding layer of the spherical support part in the entire range of operating temperatures has been investigated.

The nonlinear temperature dependence of the parameters of the contact stress-strain state is observed during deformation of the materials of the spherical support part. Mathematical temperature dependencies of the parameters of the stress-strain state and contact are established. They are suitable for analyzing the behavior of the structure over the operating temperature range. Mathematical dependencies have an average coefficient of determination $R^2 = 0.97$ and an average error size RMSE = 0.092.

AR-204 and SF-1 are promising alternatives to PTFE for molding the sliding layer.

The sliding layer from AR-204 makes it possible to obtain an improvement in the stress-strain state over the entire range of operating temperatures. The stress intensity is on average 15% less. The increase in the intensity of deformations is insignificant (less than 2%). However, at positive temperatures, the material has a greater level of movement of the end of the sliding layer than that of the Teflon sliding layer. In a similar comparison, the contact pressure is on average 3.22% higher.

SF-1 shows, on average, an increase in stresses of less than 7% with a decrease in deformations of about 2% compared to PTFE. Contact parameters are more than PTFE parameters (on average by 3–4%). However, the sliding layer has less end deformation over the entire range of operating temperatures. The maximum normal displacements of the end of the sliding layer are on average 16.6% less than that of the PTFE sliding layer.

Current studies do not give a 100% guarantee of the correct choice of rational materials of the sliding layer. This is due to the limitations of the model. Data on the temperature dependence of thermal expansion coefficients are necessary to clarify the model. Analysis of the behavior of materials during wear and aging is required to take them into account in the numerical model.

The main future studies of our scientific group are:

- Determination of the dependence of the CTE on the range of operating temperatures, including functional dependencies. Experiments are planned in 2026.
- Analysis of temperature dependencies of plastic deformation of materials and their consideration in the model, transition to elastic-viscoplastic models of material behavior.
- The formulation and conduct of experiments on the accelerated thermal aging of materials, the analysis of the influence of the time factor on the behavior of materials.

Author Contributions: Conceptualization, A.A.K., Yu.O.N., and A.P.B.; methodology, A.A.K.; software, A.A.K., A.P.B., Yu.O.N., and Yu.S.K.; validation, A.A.K., A.P.B., and Yu.O.N.; writing—original draft preparation, A.A.K., A.P.B., Yu.O.N., and Yu.S.K.; writing—review and editing, A.A.K., and Yu.S.K.; visualization, A.A.K., Yu.O.N., and A.P.B.; funding acquisition, A.P.B. All authors have read and agreed to the published version of the manuscript.

Funding: The study was supported by the Russian Science Foundation grant No. 25-29-00638, https://rscf.ru/project/25-29-00638/ (accessed on 24 May 2026).

Institutional Review Board Statement: Not applicable.

Informed Consent Statement: Not applicable.

Data Availability Statement: The original contributions presented in this study are included in the article. Further inquiries can be directed to the corresponding author.

Conflicts of Interest: The authors declare no conflict of interest.

Appendix A

Table A1. The dependence of maximum stress intensity on temperature.

Material	Mathematical relationship $\max \sigma_{int}(T)$	R^2	RMSE
PTFE	$\max \sigma_{int}(T) = 0.00288097 \cdot T^2 - 0.3301014 \cdot T + 123.86012987$	0.9997	0.0396
F4Br40M2	$\max \sigma_{int}(T) = 0.00360025 \cdot T^2 - 0.3843012 \cdot T + 126.1624975$	0.9988	0.0952
UHMWPE	$\max \sigma_{int}(T) = 0.00196553 \cdot T^2 - 0.26333566 \cdot T + 120.85105894$	0.9996	0.0384
AR-200	$\max \sigma_{int}(T) = 0.00285549 \cdot T^2 - 0.32943407 \cdot T + 123.80186813$	0.9998	0.0353
AR-202	$\max \sigma_{int}(T) = 0.00861119 \cdot T^2 - 0.68456843 \cdot T + 137.32584416$	0.9967	0.2645
AR-204	$\max \sigma_{int}(T) = 0.00473118 \cdot T^2 - 0.3170479 \cdot T + 101.51105794$	0.9059	0.6770
SF-1	$\max \sigma_{int}(T) = 0.00518052 \cdot T^2 - 0.4917043 \cdot T + 130.38761239$	0.9983	0.1439

Table A2. The dependence of the maximum strain intensity on temperature.

Material	Mathematical relationship $\max \varepsilon_{int}(T)$	R^2	RMSE
PTFE	$\max \varepsilon_{int}(T) = 0.00037793 \cdot T^2 - 0.01466551 \cdot T + 7.01811489$	0.9968	0.0074
F4Br40M2	$\max \varepsilon_{int}(T) = 0.00039321 \cdot T^2 - 0.01519178 \cdot T + 6.23571818$	0.9953	0.0093
UHMWPE	$\max \varepsilon_{int}(T) = 0.00034512 \cdot T^2 - 0.01397718 \cdot T + 8.54650889$	0.9981	0.0052
AR-200	$\max \varepsilon_{int}(T) = 0.00037757 \cdot T^2 - 0.01474905 \cdot T + 7.06867373$	0.9968	0.0074
AR-202	$\max \varepsilon_{int}(T) = 0.00039929 \cdot T^2 - 0.01634739 \cdot T + 3.98644306$	0.9864	0.0161
AR-204	$\max \varepsilon_{int}(T) = 0.00037477 \cdot T^2 - 0.00336578 \cdot T + 7.38279441$	0.9646	0.0339
SF-1	$\max \varepsilon_{int}(T) = 0.00040479 \cdot T^2 - 0.01575569 \cdot T + 5.16483127$	0.9920	0.0125

Table A3. The dependence of the maximum of contact pressure S_{cont_1} on temperature.

Material	Mathematical relationship $\max P_{cont}(T)$	R^2	RMSE
PTFE	$\max P_{cont}(T) = 0.00196824 \cdot T^2 - 0.07984176 \cdot T + 77.04723077$	0.9714	0.1162
F4Br40M2	$\max P_{cont}(T) = 0.00240437 \cdot T^2 - 0.07256109 \cdot T + 76.71681618$	0.9802	0.1228
UHMWPE	$\max P_{cont}(T) = 0.00120037 \cdot T^2 - 0.0803038 \cdot T + 77.87541059$	0.9696	0.0941
AR-200	$\max P_{cont}(T) = 0.00194881 \cdot T^2 - 0.08029565 \cdot T + 77.06744655$	0.9699	0.1183
AR-202	$\max P_{cont}(T) = 0.00545056 \cdot T^2 - 0.19647183 \cdot T + 80.8741988$	0.8732	0.7199
AR-204	$\max P_{cont}(T) = 0.00203162 \cdot T^2 - 0.14672483 \cdot T + 80.82003596$	0.9328	0.2617
SF-1	$\max P_{cont}(T) = 0.00370173 \cdot T^2 - 0.10784166 \cdot T + 77.12033766$	0.9523	0.3001

Preprints.org (www.preprints.org) | NOT PEER-REVIEWED | Posted: 26 May 2026 doi:10.20944/preprints202605.1707.v1

Table A4. The dependence of the maximum of contact shear stress S_{cont_1} on temperature.

Material	Mathematical relationship $\max \tau_{cont}(T)$	R²	RMSE
PTFE	$\max \tau_{cont}(T) = 0.00008974 \cdot T^2 - 0.00264417 \cdot T + 2.98857443$	0.9747	0.0052
F4Br40M2	$\max \tau_{cont}(T) = 0.0001093 \cdot T^2 - 0.00269705 \cdot T + 2.99675005$	0.9818	0.0056
UHMWPE	$\max \tau_{cont}(T) = 0.00006713 \cdot T^2 - 0.00312863 \cdot T + 2.99204505$	0.9313	0.0064
AR-200	$\max \tau_{cont}(T) = 0.0000888 \cdot T^2 - 0.00265594 \cdot T + 2.9893029$	0.9728	0.0053
AR-202	$\max \tau_{cont}(T) = 0.00021802 \cdot T^2 - 0.0078588 \cdot T + 3.23494905$	0.8732	0.0288
AR-204	$\max \tau_{cont}(T) = 0.00011825 \cdot T^2 - 0.00605136 \cdot T + 3.03081658$	0.9160	0.0130
SF-1	$\max \tau_{cont}(T) = 0.00015797 \cdot T^2 - 0.00449036 \cdot T + 3.05410599$	0.9259	0.0163

Table A5. The dependence of maximum normal displacement S_{cont_3} on temperature.

Material	Mathematical relationship $\max u_n(T)$	R²	RMSE
PTFE	$\max u_n(T) = 0.00001389 \cdot T^2 - 0.00014475 \cdot T + 0.07742157$	0.9896	0.0007
F4Br40M2	$\max u_n(T) = 0.00001459 \cdot T^2 - 0.00015065 \cdot T + 0.06975374$	0.9866	0.0008
UHMWPE	$\max u_n(T) = 0.00001263 \cdot T^2 - 0.00013774 \cdot T + 0.09258692$	0.9932	0.0005
AR-200	$\max u_n(T) = 0.00001385 \cdot T^2 - 0.00014535 \cdot T + 0.07788543$	0.9897	0.0006
AR-202	$\max u_n(T) = 0.00001683 \cdot T^2 - 0.00017329 \cdot T + 0.04868684$	0.9734	0.0013
AR-204	$\max u_n(T) = 0.00001167 \cdot T^2 - 0.00020402 \cdot T + 0.09128698$	0.9859	0.0010
SF-1	$\max u_n(T) = 0.00001557 \cdot T^2 - 0.00015918 \cdot T + 0.05954626$	0.9808	0.0010

References

1. Tamošaitienė, J.; Parham, S.; Sarvari, H.; Chan, D.W.M.; Edwards, D.J. A Review of the Application of Synthetic and Natural Polymers as Construction and Building Materials for Achieving Sustainable Construction. *Buildings* **2024**, *14*, 2569. https://doi.org/10.3390/buildings14082569.
2. Yurdakul, M.; Tok, M.; Döner, G.S.; Kırbıyık Kurukavak, Ç. Sustainable Polymer Composites for Automotive Industry. In: Ravindran, L., Babu, A., Meyyarappallil Sadasivan, S., Mozetič, M., Thomas, S. (eds) Macro, Micro and Nanocomposites from Sustainable Sources. *Advanced Structured Materials* **2026**, *244*, 151–173. https://doi.org/10.1007/978-981-95-2469-3_6.
3. Ramesh, M.; Manickam, T.S.; Arockiasamy, F.S.; Ponnusamy, B.; Senthilraj, S.; Chellamuthu, D.; Palanisamy, P. Revolutionizing Biomedicine: A Comprehensive Review of Polymer Composite Materials. *Eng. Proc.* **2024**, *61*, 17. https://doi.org/10.3390/engproc2024061017.
4. Zagho, M.M.; Hussein, E.A.; Elzatahry, A.A. Recent Overviews in Functional Polymer Composites for Biomedical Applications. *Polymers* **2018**, *10*, 739. https://doi.org/10.3390/polym10070739.
5. Kong, L.; Li, H.; Qi, G.; Ding, N.; Wei, B.; Zhu, W.; Zhang, Z.; Tang Y. Stability of Polymer Materials in Reinforced Thermoplastic Pipe after Actual Service in Oil Transportation System. *J. of Materi Eng and Perform* **2026**, *35*, 626-636. https://doi.org/10.1007/s11665-025-11423-y.
6. Uflyand, I.E.; Drogan, E.G.; Burlakova, V.E.; Kydralieva, K.A.; Shershneva, I.N.; Dzhardimalieva, G.I. Testing the mechanical and tribological properties of new metal-polymer nanocomposite materials based on linear low-density polyethylene and Al65Cu22Fe13 quasicrystals. *Polymer Testing* **2019**, *74*, 178-186. https://doi.org/10.1016/j.polymertesting.2019.01.004.

7. Adibnia, V.; Mirbagheri, M.; Faivre, J.; Jordan, R.; Lee, J.; Matyjaszewski, K.; Lee, D.W., Banquy, X. Bioinspired polymers for lubrication and wear resistance. *Progress in Polymer Science*, **2020**, *110*, 101298. DOI 10.1016/j.progpolymsci.2020.101298.
8. Bakhareva, V.E.; Nikolaev, G.I.; Anisimov A. Nonmetal antifriction materials for sliding friction units. *Inorganic Materials: Applied Research* **2012**, *3(6)*, 524-533. https://doi.org/10.1134/S2075113312060020.
9. Deshwal, D.; Belgamwar, S.U.; Bekinal, S.I.; Doddamani, M. Role of reinforcement on the tribological properties of polytetrafluoroethylene composites: A comprehensive review. *Polym Compos* **2024**, *45(16)*, 14475-14497. doi:10.1002/pc.28802.
10. Pretsch, T. Review on the Functional Determinants and Durability of Shape Memory Polymers. *Polymers* **2010**, *2*, 120-158. https://doi.org/10.3390/polym2030120.
11. Guay, L.; Bouaanani, N. Assessment of low temperature exposure for design and evaluation of elastomeric bridge bearings and seismic isolators in Canada. *Canadian Journal of Civil Engineering* **2016**, *43(9)*, 851-863. https://doi.org/10.1139/cjce-2015-0377.
12. Darmaev, M.V.; Ojovan, M.I.; Mashanov, A.A.; Chimytov, T.A. The Temperature Interval of the Liquid–Glass Transition of Amorphous Polymers and Low Molecular Weight Amorphous Substances. *Appl. Sci.* **2023**, *13*, 2742. https://doi.org/10.3390/app13042742.
13. Angell, C.A.; Sivarajan, S. Glass Transition. In *Reference Module in Materials Science and Materials Engineering*. Elsevier Inc.: NY, USA, 2017. DOI 10.1016/B978-0-12-803581-8.03155-6.
14. Luo, C; Pei, J.; Zhuo, W.; Niu, Y.; Li, G. Phase transition behavior and deformation mechanism of polytetrafluoroethylene under stretching. *RSC Adv.* **2021**, *11(63)*, 39813-39820. DOI 10.1039/d1ra06333b.
15. Samyn, P. Tribophysical Interpretation of Scaling Effects in Friction and Wear for Polymers. PhD Dissertation, Ghent University, Gent, Belgium, 2007.
16. Wu, J.; Wang, H.; Feng, B.; Li, Y.; Wu, S.; Yin, Q.; Yu, Z.; Huang, J. The effect of temperature-induced phase transition of PTFE on the dynamic mechanical behavior and impact-induced initiation characteristics of Al/PTFE. *Polymer Testing* **2020**, *91*, 106835. 10.1016/j.polymertesting.2020.106835.
17. Li, J.; Liu, J.; Li, W.; Peng, S.; Du, S.; Zhang, Y. Effect of temperature on the tribological properties of Polytetrafluoroethylene/Kevlar fabric/phenolic composites. *Polym. Compos.* **2023**, *44(2)*, 1280. https://doi.org/10.1002/pc.27170.
18. King, R.; Tabor, D. The effect of temperature on the mechanical properties and the friction of plastics. *Proc. Phys. Soc.* **1953**, *66*, 728. DOI 10.1088/0370-1301/66/9/302.
19. Rae, P.J.; Brown, E.N. The properties of poly(tetrafluoroethylene) (PTFE) in tension. *Polymer* **2005**, *46(19)*, 8128-8140. https://doi.org/10.1016/j.polymer.2005.06.120.
20. Krupka, J.; Dockal, K.; Krupka, I.; Hartl, M. Elastohydrodynamic Lubrication of Compliant Circular Contacts near Glass-Transition Temperature. *Lubricants* **2022**, *10*, 155. https://doi.org/10.3390/lubricants10070155
21. Yakut, A.; Yura, J. A. Parameters Influencing Performance of Elastomeric Bearings at Low Temperatures. *Journal of Structural Engineering* **2002**, *128(8)*, 986-994. DOI 10.1061/(ASCE)0733-9445(2002)128:8(986).
22. Wang, G.; Du, Y.; Zhang, C.; Li, Y. Mechanism of mechanical properties degradation of rubber isolation bearings at low temperatures. *Structures* **2025**, *71*, 108116. https://doi.org/10.1016/j.istruc.2024.108116.
23. Noade, B.M., Becker, T. Probabilistic Framework for Lifetime Bridge-Bearing Demands. *Journal of Bridge Engineering* **2019**, *24(7)*. DOI 10.1061/(asce)be.1943-5592.0001430.
24. Fu, J.; Cheng, H.; Wang, D.; Zhang, R.; Tan, X. Temperature-dependent performance of LRBs and its effect on seismic responses of isolated bridges under near-fault earthquake excitations. *Structures* **2022**, *41*, 619-628. https://doi.org/10.1016/j.istruc.2022.05.046.
25. Zhang, R.; Li, A. Experimental study on temperature dependence of mechanical properties of scaled high-performance rubber bearings. *Composites Part B: Engineering* **2020**, *190*, 107932. DOI 10.1016/j.compositesb.2020.107932.
26. Pang, H.; Jiang, T.; Dai, J.; Yang, Y.; Bai, W. Experimental Study of the Mechanical Properties of Full-Scale Rubber Bearings at 23 °C, 0 °C, and −20 °C. *Polymers* **2024**, *16*, 903. https://doi.org/10.3390/polym16070903.
27. Cardone, D.; Gesualdi, G.; Nigro, D. Effects of air temperature on the cyclic behavior of elastomeric seismic isolators. *Bulletin of Earthquake Engineering* **2011**, *9(4)*, 1227-1255. https://doi.org/10.1007/s10518-011-9244-8.

28. Hiroe, T.; Matsuo, H.; Fujiwara, K.; Tsuda, Y. Time-Temperature Equivalence for the Stress-Strain Behavior of High Density Solid Polymers. *Transactions of the Japan Society of Mechanical Engineers Series A* **1998**, *64*, 2087-2092. DOI 10.1299/kikaia.64.2087.
29. Todorov, G.; Kamberov, K.; Dimitrov, K. Inaccuracy in Structural Mechanics Simulation as a Function of Material Models. *Modelling* **2026**, *7*, 25. https://doi.org/10.3390/modelling7010025.
30. Malashin, I.P.; Tynchenko, V.S.; Nelyub, V.A.; Borodulin, A.S.; Gantimurov, A.P. Estimation and Prediction of the Polymers' Physical Characteristics Using the Machine Learning Models. *Polymers* **2024**, *16*, 115. https://doi.org/10.3390/polym16010115.
31. Uddin, M.J.; Fan, J. Interpretable Machine Learning Framework to Predict the Glass Transition Temperature of Polymers. *Polymers* **2024**, *16*, 1049. https://doi.org/10.3390/polym16081049.
32. Duan, X.; Yuan, H.; Tang, W.; He, J.; Guan, X. A General Temperature-Dependent Stress–Strain Constitutive Model for Polymer-Bonded Composite Materials. *Polymers* **2021**, *13*, 1393. https://doi.org/10.3390/polym13091393.
33. Duan, X.; Yuan, H.; Tang, W.; He, J.; Guan, X. An Engineering Prediction Model for Stress Relaxation of Polymer Composites at Multiple Temperatures. *Polymers* **2022**, *14*, 568. https://doi.org/10.3390/polym14030568
34. Doh, J.; Hur, S.H.; Lee, J. Viscoplastic parameter identification of temperature-dependent mechanical behavior of modified polyphenylene oxide polymers. *Polymer Engineering and Science* **2019**, *59*, E200-E211. https://doi.org/10.1002/pen.24910.
35. Dacol, V.; Caetano, E.; Correia, J.R. A Combined Exponential-Power-Law Method for Interconversion between Viscoelastic Functions of Polymers and Polymer-Based Materials. *Polymers* **2020**, *12*, 3001. https://doi.org/10.3390/polym12123001.
36. Nunes, S.G.; Saseendran, S.; Joffe, R.; Amico, S.C.; Fernberg, P.; Varna, J. On Temperature-Related Shift Factors and Master Curves in Viscoelastic Constitutive Models for Thermoset Polymers. *Mechanics of Composite Materials* **2020**, *56*, 573-590. https://doi.org/10.1007/s11029-020-09905-2.
37. Andrade-Campos, A.; Thuillier, S.; Pilvin, P.; Teixeira-Dias, F. On the determination of material parameters for internal variable thermoelastic-viscoplastic constitutive models. *International Journal of Plasticity* **2007**, *23(8)*, 1349-1379. https://doi.org/10.1016/j.ijplas.2006.09.002.
38. Halamka, J.; Bartošák, M. Use of machine learning in determining the parameters of viscoplastic models. *Engineering Computations* **2025**, *42(6)*, 1927–1941. https://doi.org/10.1108/EC-02-2024-0166.
39. Meißner, P.; Hoppe, T.; Vietor, T. Comparative Study of Various Neural Network Types for Direct Inverse Material Parameter Identification in Numerical Simulations. *Appl. Sci.* **2022**, *12*, 12793. https://doi.org/10.3390/app122412793
40. Alaraby, M.; Abass, D.; Velázquez, A.; Hernández, A.; Marcos, R. Polytetrafluoroethylene microplastic properties, pollution, toxicity and analysis: a review. *Environmental Chemistry Letters* **2025**. https://doi.org/10.1007/s10311-025-01885-w
41. Liang, X.; Wu, P.; Lan, L.; Wang, Y.; Ning, Y.; Wang, Y.; Qin, Y. Effect of Polytetrafluoroethylene (PTFE) Content on the Properties of Ni-Cu-P-PTFE Composite Coatings. *Materials* **2023**, *16*, 1966. https://doi.org/10.3390/ma16051966
42. Bosq, N.; Guigo, N.; Persello, J.; Sbirrazzuoli, N. Crystallization of Polytetrafluoroethylene in a Wide Range of Cooling Rates: Nucleation and Diffusion in the Presence of Nanosilica Clusters. *Molecules* **2019**, *24*. 1797. https://doi.org/10.3390/molecules24091797
43. Maculotti, G.; Goti, E.; Genta, G.; Mazza, L.; Galetto, M. Comprehensive mechanical and tribological characterization of metal-polymer PTFE+Pb/Bronze coating by in-situ electrical contact resistance measurement augmented tribo-mechanical tests. *Tribology International* **2024**, *193*, 109397. https://doi.org/10.1016/j.triboint.2024.109397
44. Carvalho, P.R.P.; Coda, H.B.; Sanches, R.A.K. A large strain thermodynamically-based viscoelastic–viscoplastic model with application to finite element analysis of polytetrafluoroethylene (PTFE). *European Journal of Mechanics—A/Solids* **2023**, *97*, 104850. https://doi.org/10.1016/j.euromechsol.2022.104850.

45. Liu, F.; Jin, Y.; Li, J.; Jiang, W.; Zhao, W. Improved coefficient thermal expansion and mechanical properties of PTFE composites for high-frequency communication. *Composites Science and Technology* **2023**, *241*, 110142. https://doi.org/10.1016/j.compscitech.2023.110142
46. Rondinella, A.; Andreatta, F.; Turrin, D.; Fedrizzi, L. Degradation Mechanisms Occurring in PTFE-Based Coatings Employed in Food-Processing Applications. *Coatings* **2021**, *11*, 1419. https://doi.org/10.3390/coatings11111419
47. Bogdanova, A.P.; Kamenskikh, A.A.; Muhametshin, A.R.; Nosov, Y.O. Numerical Modeling of Thermomechanics of Antifriction Polymers in Viscoelastic and Elastic-Viscoplastic Formulations. *Applied Mechanics* **2026**, *7*, 2. https://doi.org/10.3390/applmech7010002
48. Adamov, A.A.; Keller, I.E.; Ostrer, S.G.; Seletkov, D.V. Evaluation of the Performance of Antifriction PTFE Composites at a Pressure Over 60 MPA. I. Comparison of Their Hardness and Deformation Properties Under Free and Constrained Compression. *Mechanics of Composite Materials* **2022**, *58(5)*, 673-688. DOI 10.1007/s11029-022-10058-7
49. Adamov, A.A.; Keller, I.E.; Petukhov, D.S.; Kuzminykh, V.S.; Patrakov, I.M.; Grakovich, P.N.; Shilko, I.S. Evaluation of the Performance of PTFE-Composites as Antifriction Layers in Supporting Parts with a Spherical Segment. *J. Frict. Wear* **2023**, *44*, 127–134. https://doi.org/10.3103/S1068366623030029.
50. Kamenskikh, A.A.; Bogdanova, A.P.; Nosov, Y.O.; Kuznetsova, Y.S. Influence of the Pattern of Coupling of Elements and Antifriction Interlayer Thickness of a Spherical Bearing on Structural Behavior. *Designs* **2025**, *9*, 117. https://doi.org/10.3390/designs9050117.
51. Sun, Y.; Deng, W.; Wang, H.; Jian, R.; Bai, W.; Chu, D.; Hou, P.; He, Y. Machine-Learning-Assisted Viscoelastic Characterization of PC/ABS Blends via Multi-Frequency Dynamic Mechanical Analysis. *Polymers* **2026**, *18*, 599. https://doi.org/10.3390/polym18050599.
52. Ciganas, J.; Kalinauskis, T.; Cigane, U. Thermo-Mechanical and Fatigue Behavior of 3D-Printed PA12 CF15 for Engineering Application. *Polymers* **2026**, *18*, 563. https://doi.org/10.3390/polym18050563.
53. Umair, M.; Ullah, T.; Abbas, A.; Nawab, Y.; Seyam, A.-F.M. Dynamic Mechanical Performance of 3D Woven Auxetic Reinforced Thermoplastic Composites. *J. Compos. Sci.* **2025**, *9*, 649. https://doi.org/10.3390/jcs9120649.
54. Padhy, V.; Kandasubramanian, B. Polymer nanocomposites of ultra-high molecular weight polyethylene. *Polymer Bulletin* **2024**, *81*, 15259-15292. https://doi.org/10.1007/s00289-024-05439-y.
55. Huber, P.; Bresler, M.; Paroli, L.; Kruzel, U. Seismic Isolation Protection System for the 1081-Bed Eskisehir City Hospital in Turkey. Synergy of Culture and Civil Engineering—History and Challenges, Wrocław, Poland, 7-9 October 2020. *IABSE Symposium Wroclaw* **2020**, 773-780. doi 10.2749/wroclaw.2020.0773.
56. Zhao, F.; Zheng, X.; Zhou, S.; Zhou, B.; Xue, S.; Zhang, Y. Constitutive model for epoxy shape memory polymer with regulable phase transition temperature. *International Journal of Smart and Nano Materials* **2021**, *12(1)*, 72–87. https://doi.org/10.1080/19475411.2021.1876176
57. Smetannikov, O.Y.; Faskhutdinova, Y.B.; Ilinyh, G.V. Identification of a Thermoviscoelastic Crosslinked Polymer Model Taking into Account Large Deformations and its Application. *Mech. Solids* **2025**, *60*, 4434–4449. https://doi.org/10.1134/S0025654425601466.
58. Trufanov, A.N.; Kamenskikh, A.A.; Lesnikova, Y.I. Thermomechanics and Thermophysics of Optical Fiber Polymer Coating. *Polymers* **2026**, *18*, 271. https://doi.org/10.3390/polym18020271.
59. Schuster, M.; Härth, M.; Thiele, K.; Bennison S.J. Quantification of the linear viscoelastic behavior of multilayer polymer interlayers for laminated glass. *Glass Structures & Engineering* **2023**, *8*, 457–469. https://doi.org/10.1007/s40940-023-00229-w.
60. Zhang, J.; Zhu, T.; Deng, X.; Liu, X.; Xiao, R.; Zhang, C.; Wang, L. Solution of 3D elastic frictionless contact problem by DiBFM based on local adaptive mesh refinement. *Engineering Analysis with Boundary Elements* **2025**, *181*, 106531, https://doi.org/10.1016/j.enganabound.2025.106531.
61. Zhou, X.-W.; Jin, Y.-F.; Yang, J.; Yin, Z.-Y.; Liu, F.-T.; Chen, X. A mixed smoothed finite element limit analysis framework: integrating non-conforming mesh and cohesive-frictional contact. *Computer Methods in Applied Mechanics and Engineering* **2026**, *449(A)*, 118510. https://doi.org/10.1016/j.cma.2025.118510.

 doi:10.20944/preprints202605.1707.v1

62. Danielson, K.T. Curved node-to-face contact schemes for higher-order finite elements in lumped-mass explicit methods. *Computer Methods in Applied Mechanics and Engineering* **2022**, *395*, 115056. https://doi.org/10.1016/j.cma.2022.115056.
63. Kamenskih, A.A.; Trufanov, N.A. Regularities of interactions between elements of a spherical contact unit with an antifriction polymeric interlayer. *J. Frict. Wear* **2015**, *36*, 170–176. https://doi.org/10.3103/S1068366615020075.
64. Wriggers, P.; Korelc, J.; Junker, Ph. A third medium approach for contact using first and second order finite elements. *Computer Methods in Applied Mechanics and Engineering* **2025**, *436*, 117740. https://doi.org/10.1016/j.cma.2025.117740.
65. Wriggers, P.; Korelc, J.; Junker, P. First order finite element formulations for third medium contact. *Comput Mech* **2025**, *76*, 829–845. https://doi.org/10.1007/s00466-025-02628-y.
66. Bogdanova A.P., Kamenskikh A.A., Muhametshin A.R., Nosov Y.O. Numerical Modeling of Thermomechanics of Antifriction Polymers in Viscoelastic and Elastic-Viscoplastic Formulations. *Applied Mechanics* **2026**, *7*, 2. https://doi.org/10.3390/applmech7010002
67. Nosov Y.O., Kamenskikh A.A. Influence Analysis of Lubricant Recesses on the Working Capacity of the Bridge Span Spherical Bearing. *Lubricants* **2022**, *10*, 283. https://doi.org/10.3390/lubricants10110283
68. Wei, B.; Wang, X.; Cao, S.; Jiang, L.; Yang, Z. Research on friction-type bearings for high-speed railway bridges based on the concept of quasi-isolation. *Engineering Structures* **2025**, *328*, 119674. https://doi.org/10.1016/j.engstruct.2025.119674.
69. Deng, N.; He, M.; Gu, N.; Liang, H. Design and Performance Research of a New Type of Spherical Force-Measuring Bearing of Bridges Based on Button Type Microsensor. *KSCE Journal of Civil Engineering* **2024**, *28*, 5066–5076. https://doi.org/10.1007/s12205-024-2646-3.
70. Adamov, A.A.; Kamenskikh, A.A.; Pankova, A.P. Influence Analysis of the Antifriction Layer Materials and Thickness on the Contact Interaction of Spherical Bearings Elements. *Lubricants* **2022**, *10*, 30. https://doi.org/10.3390/lubricants10020030
71. Guo, J.; Geng, T.; Yan, H.; Du, L.; Zhang, Z.; Sun, C. Implementation of a Load Sensitizing Bridge Spherical Bearing Based on Low-Coherent Fiber-Optic Sensors Combined with Neural Network Algorithms. *Sensors* **2021**, *21*, 37. https://doi.org/10.3390/s21010037.
72. Li, S.; Zhang, Z.; Gan, L.; Yin, J.; Fu, M. Design and Monitoring Application of an Adjustable Intelligent Bearing Based on Pressure Sensing. *Sensors* **2024**, *24*, 7820. https://doi.org/10.3390/s24237820.
73. Wang, J.; Wu, D.; Guo, J. Long-term force-measurement for bridge smart bearing capable of in-situ calibration. *Measurement* **2026**, *275*, 121301. https://doi.org/10.1016/j.measurement.2026.121301.
74. Chen, S.; Zhou, Y.; Xie, K.; Zhang, P.; Li, C. Dynamic Adaptability of Spherical Bearings in Small-Span Bridges for Heavy-Haul Railways. *Buildings* **2025**, *15*, 619. https://doi.org/10.3390/buildings15040619.
75. Masi, A.; Santarsiero, G.; Savoia, M.; Cardillo, E.; Belletti, B.; Macaluso, R.; Orlando, M.; Menichini, G.; Morano, G.; Marano, G.C.; et al. Development of a Large Database of Italian Bridge Bearings: Preliminary Analysis of Collected Data and Typical Defects. *Infrastructures* **2025**, *10*, 69. https://doi.org/10.3390/infrastructures10030069.
76. Kromanis, R.; Kripakaran, P.; Harvey, B. Long-term structural health monitoring of the Cleddau bridge: evaluation of quasi-static temperature effects on bearing movements. *Structure and Infrastructure Engineering* **2015**, *12(10)*, 1342–1355. https://doi.org/10.1080/15732479.2015.1117113.
77. Deng, N.; Zhang, H.; Ning, F.; Tang, Z. Research on the Mechanical Properties and Temperature Compensation of an Intelligent Pot Bearing for a Pipe-Type Welding Strain Gauge. *Sensors* **2023**, *23*, 9648. https://doi.org/10.3390/s23249648
78. Yu, X.; Yuan, Y.; Wang, S.; Deng, Z. Innovative castable polyurethane elastomer bearing system for highway bridges: Mechanical properties and performance evaluation. *Construction and Building Materials* **2025**, *490*, 142494. https://doi.org/10.1016/j.conbuildmat.2025.142494.